2013

NOVEL G-QUADRUPLEX BINDERS WITH POTENTIAL FOR A DUAL DNA CROSS-LINKING MECHANISM OF ACTION

Nathan S. Duncan
The University of Montana

NOVEL G-QUADRUPLEX BINDERS WITH POTENTIAL FOR A DUAL DNA CROSS-LINKING MECHANISM OF ACTION

By

NATHAN S. DUNCAN

B.S. Biochemistry, Missouri Southern State University, Joplin, Missouri, 2010

Thesis

presented in partial fulfillment of the requirements
for the degree of

Master of Science
in Medicinal Chemistry

The University of Montana
Missoula, Montana

May 2013

Approved by:

Sandy Ross, Dean of The Graduate School
Graduate School

Nicholas R. Natale, Director, Medicinal Chemistry Program
Department of Biomedical and Pharmaceutical Sciences

Howard D. Beall
Department of Biomedical and Pharmaceutical Sciences

Michael R. Braden
Department of Biomedical and Pharmaceutical Sciences

Orion B. Berryman
Department of Chemistry & Biochemistry

"Novel G-quadruplex Binders with Potential for a Dual DNA

Cross-Linking Mechanism of Action"

Chairperson: Nicholas R. Natale

Co-Chairperson: Howard D. Beall, Michael R. Braden, Orion B. Berryman

Genomic DNA is organized around the double-stranded of B-form DNA, which is both durable and flexible enough to store and pass on genetic information. Once freed from the associations of an extended complimentary sequence, single stranded DNA and RNA can adopt a vast array of stable secondary structure motifs, such as stem-loop, pseudo-knots, and tetra-loops, ideal for its involvement in biological settings other than as a store of genetic information. Originally, alkylating agents were used as "mustard gas" and related chemical weapons in World War I. Alkylating agents, in general, can react with one or two different 7-N-guanine residues and could potentially result in the cross-linkage of DNA strands, preventing uncoiling of the DNA double helix leading to cell death. More recent evidence show that guanine-rich nucleic acids can fold into distinctive four-stranded conformers found in telomeric DNA repeats (i.e. TTAGGG), also known as G-quadruplexes (G4), as well as in sequences in the promoter and other regulatory regions of genes, especially those involved in cellular proliferation. Small molecules that induce the formation of, and selectively bind to, G4 structures are of interest for development as potential anticancer therapeutics. Novel 10-oxoanthracene and substituted anthracenyl isoxazole esters (AIEs) were synthesized and characterized based on NMR studies. To date, quarfloxin is the only G-quadruplex ligand from the large number developed to progress to clinical evaluation. The synthesis, structural characterization, and biological studies will be presented.

ACKNOWLEDGEMENT

First of all I would like to thank all those who have contributed to this work throughout their efforts to evaluate and characterize the biological activity of the compounds which I have synthesized, including Dr. Andrea Stierle and Dr. Don Stierle. I would also like to thank the Department of Biomedical and Pharmaceutical Sciences for providing me with the outstanding educational opportunity and resources to complete my thesis. I extend my heartfelt appreciation to the members of my dissertation committee: Dr. Natale, Dr. Beall, Dr. Braden, and Dr. Berryman. I would especially like to express my gratitude to my mentor, Dr. Nick R. Natale for his patience and guidance in helping me to complete this project throughout the past years. Finally I am grateful for the support of my family including my parents, my brother, my sister and above all my wife Laura for her patience and fortitude.

TABLE OF CONTENTS

List of Figures

List of Schemes

1.1 Introduction

Gellert, Lipsett and Davies were the first to initially identify four-stranded helical arrangements in fibers of guanosine monophosphate in 1962, which would have made last year, 2012, the 50th anniversary of the birth of the quadruplex field.[1] Genomic DNA, which is organized around double-stranded B-form DNA, is both durable and flexible enough to store and pass on genetic information. The standard of several secondary structural motifs, helical B-form DNA, utilizes an anti-parallel arrangement of two complimentary strands, stabilized by Watson-Crick base pairing (Figure 1). Once

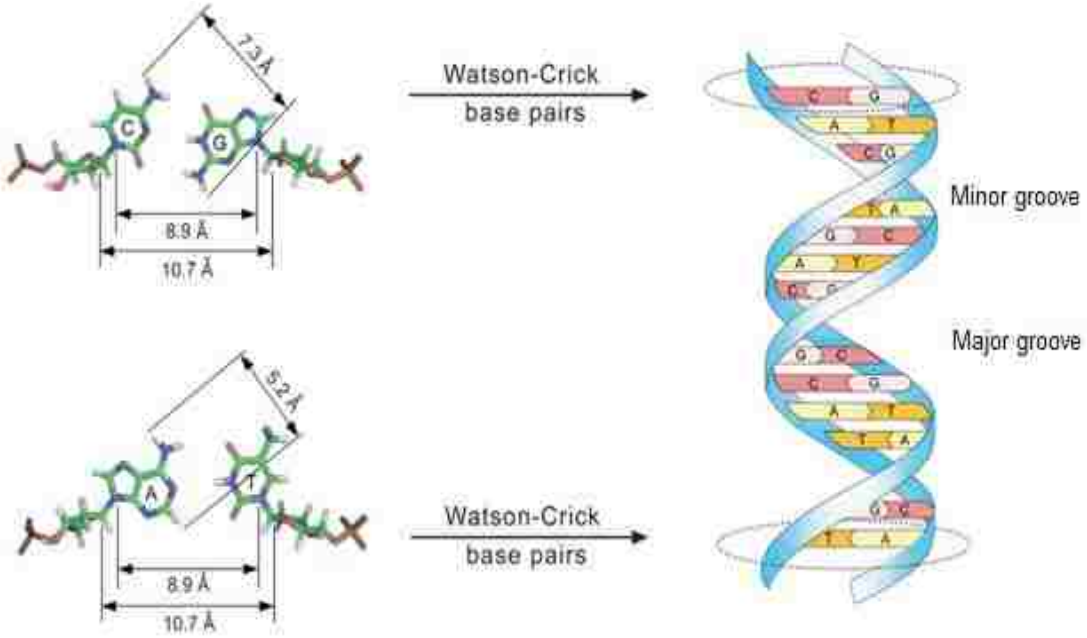

Figure 1. The dimensions of duplex DNA and its base pair surface. Reprinted from reference [6] with permission from the publisher.

freed from the associations of an extended complimentary sequence, single stranded DNA and RNA can adopt a vast array of other stable secondary structure motifs, such as stem-loop, pseudo-knots, and tetra-loops, ideal for its involvement in other biological settings other than as a store of genetic information.[2] Guanine-rich nucleic acids can fold

into distinctive four-stranded conformers found in telomeric DNA repeats (i.e. TTAGGG) as well as in sequences in the promoter and other regulatory regions of genes, especially those involved in cellular proliferation. [3, 4] The terminal 3'-telomeric 150–250 nucleotides single-stranded DNA can be induced and stabilized by certain small molecules to form higher order G-quadruplex structures (Figure 2) that prevent the interaction and regulation of the telomerase enzyme complex (Figure 3) in cancer cells

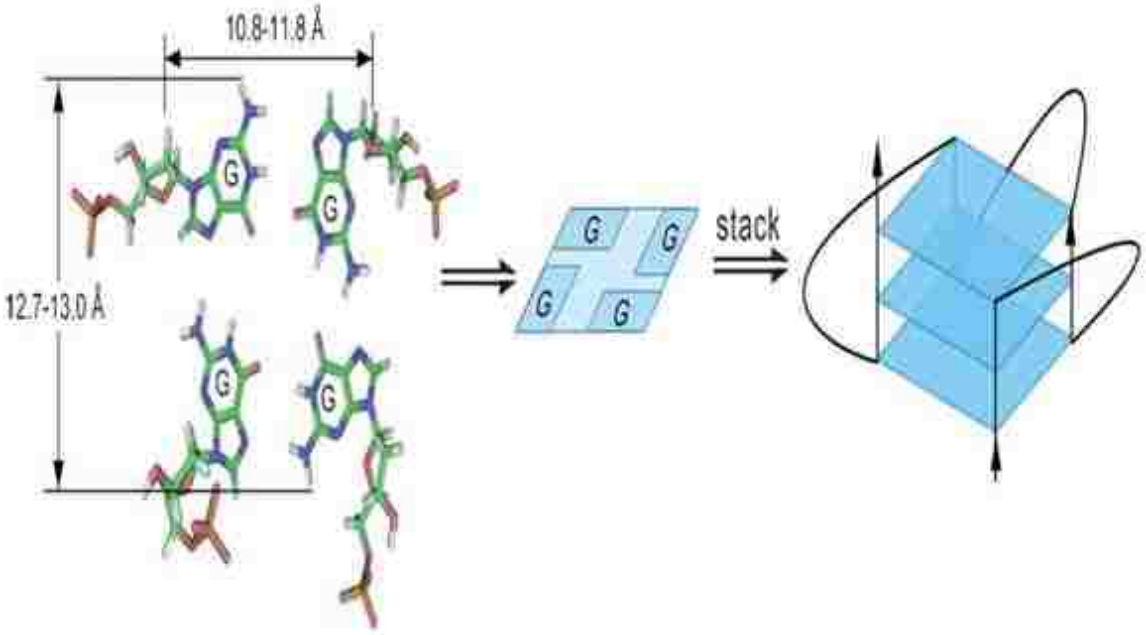

Figure 2. G-Quadruplex structure and G-quartet surface. Reprinted from reference [6] with permission from the publisher.

(which is over-expressed in ~80–90% [4-6]), and thereby maintain telomere length homeostatis (acting as a tumor promoter). Loss of the telomerase enzyme deprotects the telomeres and initiates DNA damage-response mediated cell death since the enzyme can no longer synthesize any further telomeric DNA repeats (Figure 3).[3, 4, 7, 8] G-rich sequences can utilize both the Watson-Crick and Hoogsteen faces of a guanine base to self-associate in a hydrated environment containing cations to form extended four

stranded stacked structures termed G-quadruplex or G-quartet (Figure 2). The stability of extended quadruplexes has fuelled research beyond biology into the development of nano wires and sensors.[2, 9, 10]

Quadruplex formation at the telomeric single-strand overhang (Figure 3) may itself be a DNA damage signal, producing responses analogous to those of other mediators of telomere damage. The biological function of induced telomeric quadruplexes remains to be fully clarified; an end-protective role has been suggested.[11-13] However, to date, there is no direct evidence of a role for telomeric G-quadruplexes in the functioning of telomeres in normal human cells.[4] The working hypothesis is that the ligand stabilizes telomeric DNA into quadruplex structures that inhibit the primer from interacting as a single stranded species with the RNA template of telomerase. The approach to target quadruplexes overrides the problem of telomerase resistance along with inhibiting telomere-independent mechanisms of telomere maintenance in cancer cells, making them more universally applicable than conventional telomerase inhibitors.[2, 10]

The discrete structures formed by defined numbers of guanosine nucleotides have been subsequently termed quadruplexes, a name that is now applied to any structural arrangement that incorporates at least two G-quartets (Figure 2)[14] together with the intervening sequences that hold the quartets together. For some years the quadruplex field lay dormant, with the widespread belief that these structures were at best artifacts, without functional biological significance. It has been only in the past 15 years that this picture has been dispelled, with an ever-increasing number of studies indicating a diversity of biological roles for quadruplex nucleic acids, at least some of which have

therapeutic implications. This worldwide increase in activity has resulted in a tenfold increase in the number of publications on quadruplexes; with over 400 in 2011. The more general interest in quadruplexes has been shown by almost 12,000 citations in 2011 to the quadruplex literature. [1, 15]

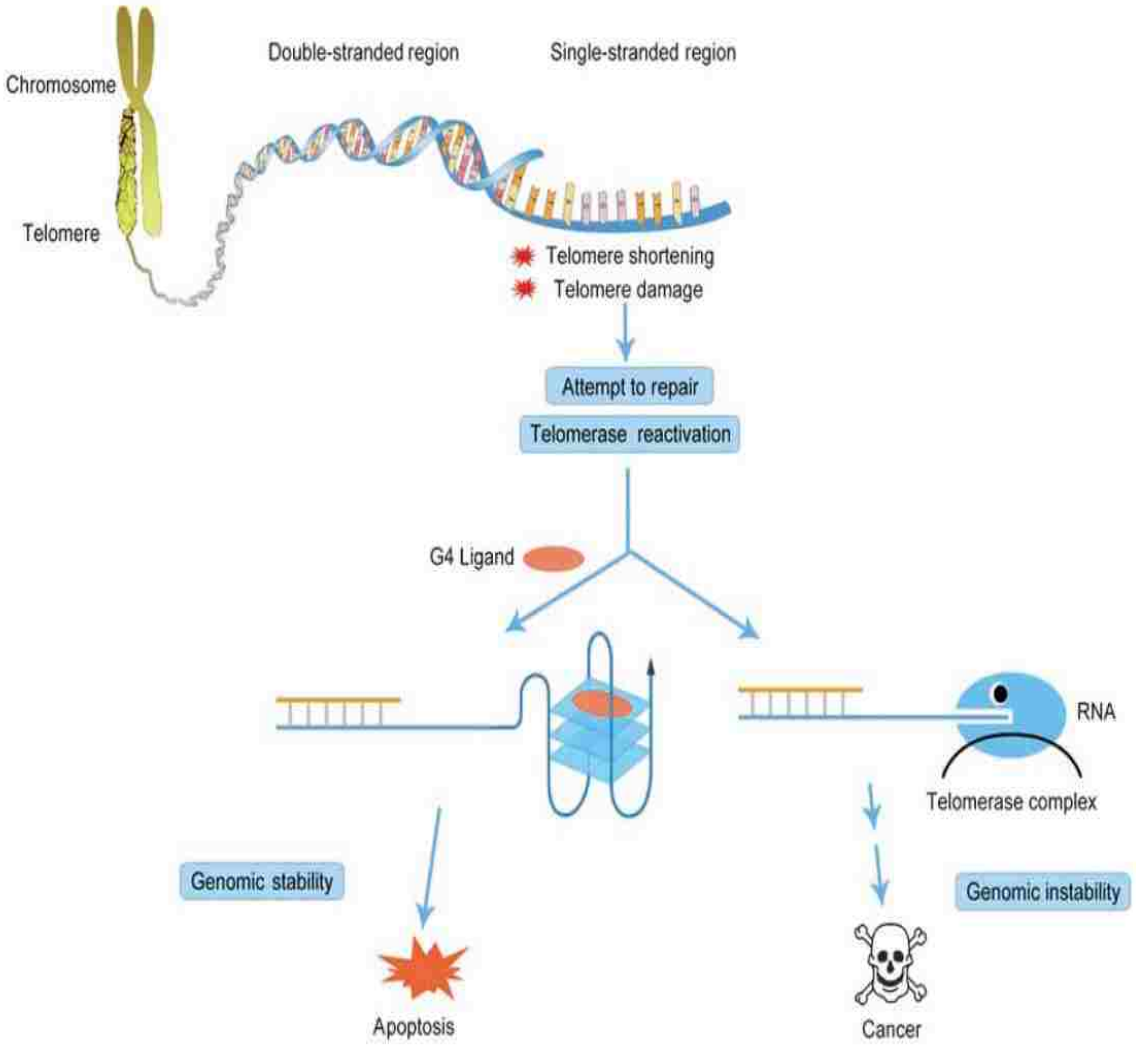

Figure 3. Biological roles and structure of telomeres and the telomerase enzyme. Reprinted from reference [6] with permission from the publisher.

The prevalence of G-quadruplex forming-sequences in the promoter regions of genes involved in proliferation such as c-myc, c-kit, k-ras, bcl-2 and PDGF-A suggests

that it might be possible to use them to artificially regulate transcription of these genes, and there is growing evidence that this is achievable. Even though G-quadruplex formation has to compete with stable duplex DNA formed at promoter sites, it has been shown that G-quadruplexes can be induced under conditions which mimic the intracellular environment, and that their formation can have significant biological consequences.[3] Telomerase activity and G4-DNA formation in telomeres are significant as they represent potential sites for small molecule drug interactions, in the treatment of cancer, which may not have the ill effects of indiscriminate B-DNA binding. Small molecules that can selectively bind to and stabilize these G-DNA structures would represent a new class of potential anti-cancer therapeutics. [16-18]

2.1 B-DNA Characteristics

2.1.1 DNA-Interactive Drugs

Another site in which drugs can interact is with DNA or deoxyribonucleic acid, the polynucleotide that carries the genetic information in cells. Because DNA is so vital to human functioning, and from the perspective of medicinal chemistry the overall shape and chemical structure of DNA found in normal and abnormal cells is nearly indistinguishable, drugs that interact with DNA are generally very toxic to normal cells. Because the medical term for cancer is *neoplasm*, anticancer drugs may be referred to as *antineoplastic agents*. Unlike the design of drugs that act on enzymes in a foreign organism, there is little that is useful to direct the design of selective agents against abnormal DNA. One feature of cancer cells that differentiates them from that of most normal cells is that cancer cells undergo a rapid, abnormal, and uncontrolled cell division. Genes coding for differentiation in cancer cells appear to be shut off or inadequately

expressed, while genes coding for cell proliferation are expressed when they should not be. Because these cells are continually undergoing mitosis, there is a constant need for rapid production of DNA. Because of the correspondence of normal and abnormal DNA, a compound that reacts with a cancer cell will react with a normal cell as well. However, because of rapid cell division, cancer cell mitosis can be halted preferentially to that found in normal cells where there is sufficient time for the triggering of repair mechanisms. Tumor cells, however, are defective in their ability to undergo cell cycle arrest or apoptosis in response to DNA damage. Cancer cells that cannot undergo cell cycle arrest are sensitive to DNA damaging agents. In general, anticancer drugs are most effective against malignant tumors with a large proportion of rapidly dividing cells, such as leukemias and lymphomas. Unfortunately, the most common tumors are solid tumors, which have a small proportion of rapidly dividing cells.[19]

2.1.2 Structure of DNA

The elucidation of the structure of DNA by Watson and Crick (Figure 1) was the culmination of experimental results reported by a large number of scientists over several years. All of this data was digested by Watson and Crick, who then proposed that two strands of DNA are intertwined into a helical duplex which is held together by specific hydrogen bonding between base pairs of adenine with thymine and guanine with cytosine (Figure 4) to explain the results of Gulland and Chargar and that there base pairs were stacked at 3.4Å distance, as observed in the X-ray photographs. Furthermore, right-handed rotation between adjacent base pairs by about 36° produces a double helix with 10 base pairs per turn. A model of the helix was constructed using dimensions and confirmations of the individual nucleotides based on the structure of cytidine. The bases

are located along the axis of the helix with sugar phosphate backbones winding in an antiparallel orientation along the periphery (Figure 1). [19]

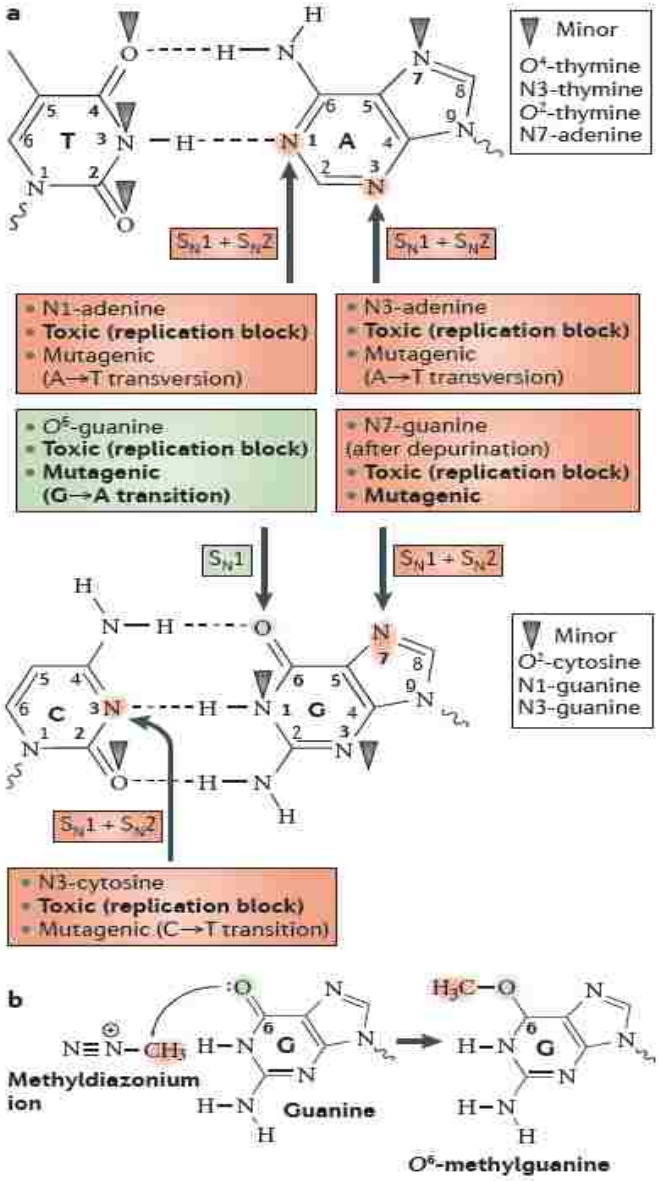

Figure 4. Sites of alkylation on DNA bases. Reprinted from reference [21] with permission from the publisher.

All of the bases of the DNA are on the inside of the double helix, and the sugar phosphates are on the outside; therefore, the bases on one strand are close to those on the other. Because of this fit, specific base pairing between a large purine base (either A or

G) on one chain and a smaller pyrimidine base (T or C) on the other chain are essential. Hydrogen bonds between guanines and cytosine or adenine and thymine are more effective than any other combination. Therefore, *complementary base pairs* (also called *Watson-Crick base pairs*) form between guanines and cytokines or adenines and thymines only, resulting in a complementary relation between sequences of bases on the two polynucleotide strands of the double helix. As you might predict, because there are three hydrogen bonds between G and C base pairs and only two hydrogen bonds between A and T base pairs, the former are more stable. [19]

The two glycoside bonds that connect the base pair to its sugar rings are not directly opposite each other, and, therefore, the two sugar-phosphate backbones of the double helix are not equally spaced along the helical axis (Figure 1). As a result, the grooves that are formed between the backbones are not of equal size. The larger groove is called the *major groove* and the smaller one is called the *minor groove* (Figure 1). One side of every base pair faces into the major groove, and the other side faces into the minor groove. The floor of the major groove is filled with base pair nitrogen and oxygen atoms that project inward from their sugar phosphate backbones toward the center of the DNA. The floor of the minor groove is filled with nitrogen and oxygen atoms of base pairs that project outward from their sugar phosphate backbones toward the outer edge of the DNA.[19]

2.1.3 Classes of Drugs That Interact with DNA

In general, there are three major classes of clinically important DNA-interactive drugs: *reversible binders*, which interact with DNA through the reversible formation of non-covalent interactions; a*lkylators*, which react covalently with DNA bases; and *DNA*

strand breakers, which generate reactive radicals that produce cleavage of the polynucleotide strands. It is not yet clear what DNA sequences (genes) should be targeted. Also, in traditional cancer chemotherapy significant amounts of DNA damage are required to elicit the cell killing that is necessary for effective anticancer drugs. [19]

Alkylating agents are a ubiquitous family of reactive chemicals that transfer alkyl carbon groups onto a broad range of biological molecules, thereby altering their structure and potentially disrupting their function as Lippard *et. al* showed with cisplatin[20] (Figure 5). Alkylating agents are generally unavoidable owing to their abundant presence in the

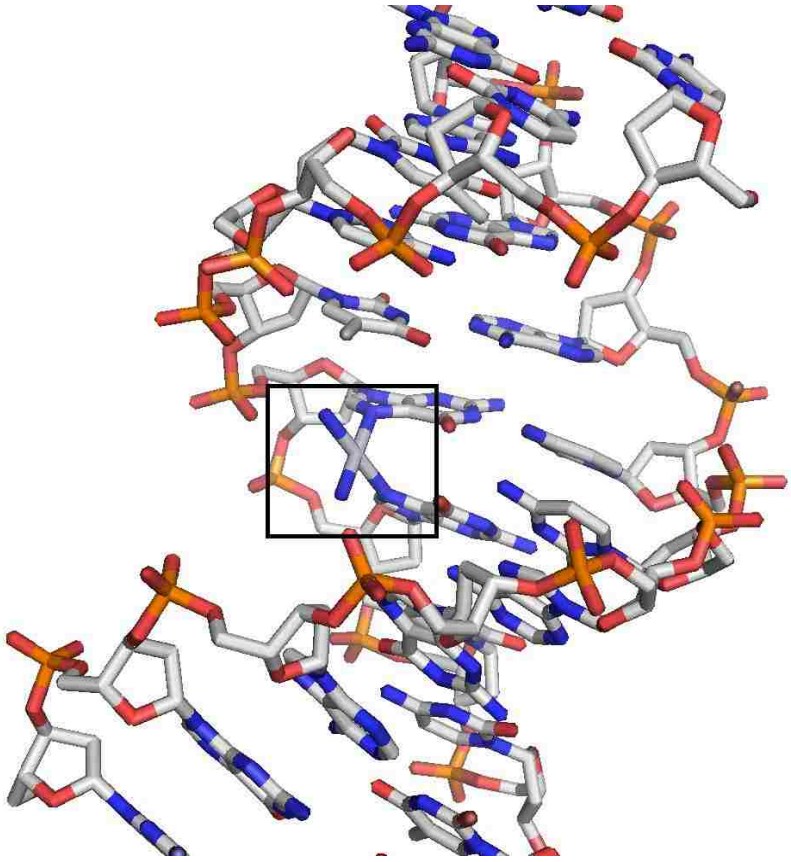

Figure 5. Structure of the damaged DNA duplex

environment and within living cells. Major sources of external alkylating agents include the constituents of air, water and food, such as biological byproducts (for example,

abiotic plant material) and pollutants (for example, tobacco smoke and fuel combustion products). Internally, alkylating agents can arise as byproducts of oxidative damage or from cellular methyl donors such as *S*-adenosylmethionine. Owing to the cytotoxic, teratogenic and carcinogenic effects that are caused by alkylation damage, alkylating agents pose considerable threats to human health. In spite of this, certain toxic alkylating agents are commonly used systemically as chemotherapeutic drugs in cancer patients, with the goal of killing cancer cells. Consequently, although alkylating agents can induce cancer, they are also used to treat cancer. On the basis of the double-edged properties of alkylating agents, a greater understanding of the cellular factors that determine biological outcome in response to alkylation damage is particularly relevant for both cancer prevention and cancer therapy, in addition to general human health. The biological response to alkylating agents can be complex owing to the variety of lesions that are introduced by a single alkylating agent in combination with the diversity of cellular repair mechanisms and response pathways that can be elicited on alkylation damage.[21]

2.1.4 DNA Alkylators

Alkylating agents react with the ring nitrogens (N) and extracyclic oxygen (O) atoms of DNA bases (Figure 1) to generate a variety of covalent adducts that range from simple methyl groups to complex alkyl additions. The pattern of DNA lesions generated by an alkylating agent depends on the number of reactive sites within the alkylating agent (monofunctional versus bifunctional), its particular chemical reactivity (SN_1-type versus SN_2-type nucleophilic substitution) (Scheme 1a), the type of alkyl group addition (methyl or chloroethyl and so on) and the DNA substrate (double-stranded or single-stranded). Monofunctional alkylating agents contain one active chemical moiety for the

modification of a single site in DNA, whereas bifunctional alkylating agents contain two reactive groups that can bond to separate DNA bases to form interstrand crosslinks. Whereas SN_2-alkylating agents mainly target ring nitrogen atoms in DNA bases, SN_1-alkylating agents can modify these nitrogens plus the extracyclic oxygen groups (Figure 6). Notably, nearly all chemotherapeutic alkylating drugs that are currently used in the clinic are SN_1-type and they can be either mono-functional or bi-functional (Figure 6). [21]

Owing to the high nucleophilic reactivity of the N7-position of guanine in DNA, most monofunctional methylating agents induce the formation of N7-methyl guanine (7meG) as the predominant methylation adduct, which accounts for 60–80% of the total alkylation lesions in DNA with 3meA being second accounting for 10–20% (Figure 4). By itself, 7meG does not possess any mutagenic or cytotoxic properties with 3meA lesion being highly cytotoxic. Amongst the oxygen atoms of DNA, the O6-position of guanine is a major site of methylation by SN_1-type alkylating agents for generating O6-methylguanine (*O*6meG) (Figure 4). Even though *O*-alkyl lesions are generated to a much lesser extent than N-alkyl adducts, the induction of O6meG lesions by alkylating agents is of great biological relevance because O6meG can readily mispair with thymine during DNA replication to cause many of the mutagenic and cytotoxic biological effects of alkylating agents. Alkylating agents can also modify other nitrogen and oxygen atoms in DNA to generate additional toxic and mutagenic lesions. However, these lesions are observed at tenfold to 100-fold lower levels than the lesions mentioned above and represent a small proportion of total alkylation adducts. [21]

Several monofunctional SN_1-methylating agents are currently used as anticancer drugs; these include the triazine family of compounds such as dacarbazine, procarbazine

and temozolomide, as well as the nitrosourea compound streptozotocin (Figure 6). Owing to their chemical reactivity as monofunctional SN_1-methylating agents, these

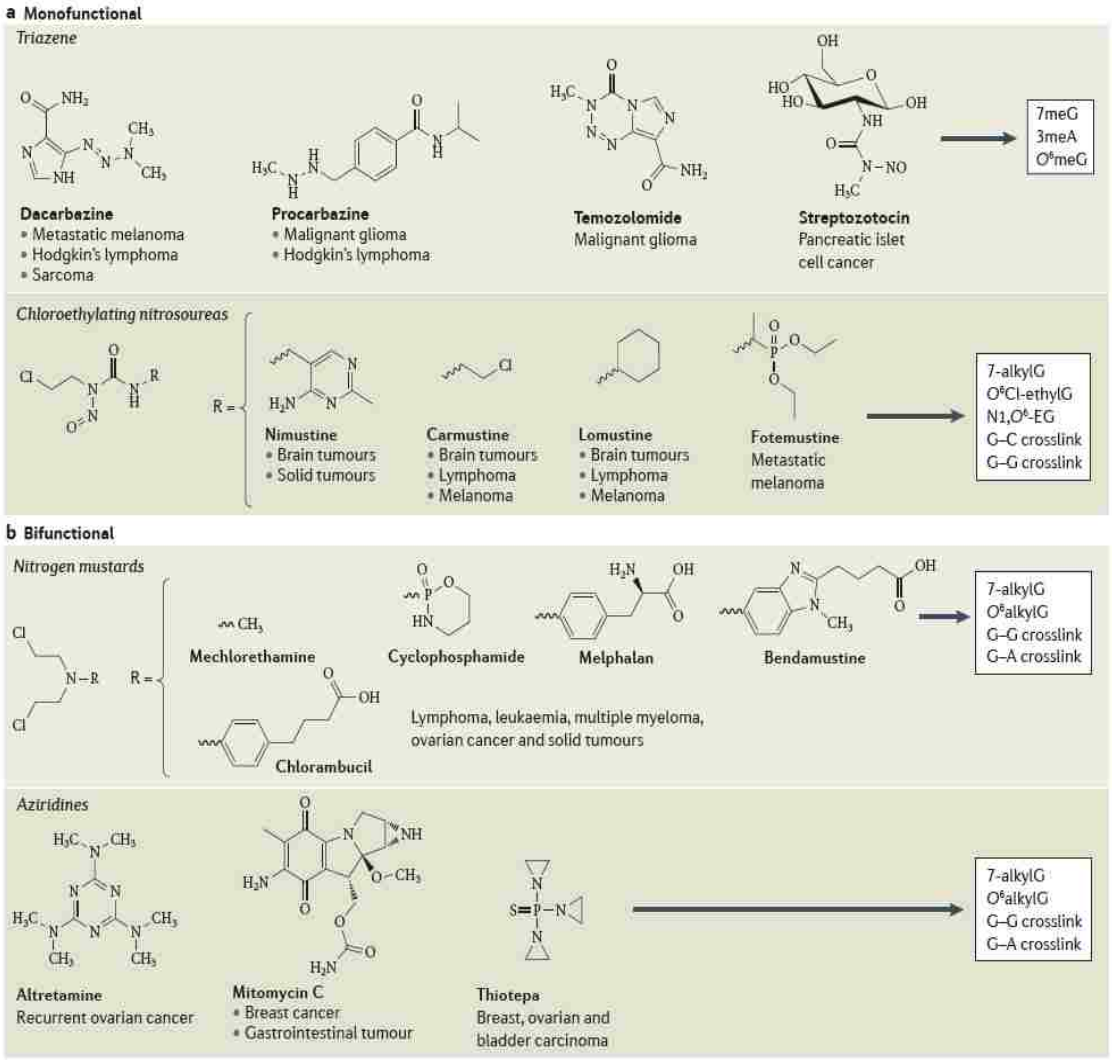

Figure 6. DNA lesions induced by alkylating agents. Reprinted from reference [21] with permission from the publisher.

chemotherapeutic alkylating agents produce substantial levels of 7meG, 3meA and O6meG as the primary alkylated DNA adducts. The chloroethylating agents represent another major class of monofunctional alkylating agents that react with DNA at a similar specificity to SN_1-methylating agents except with the addition of a chloroethyl group.

Most nitrosourea compounds that are used in the clinic are chloroethylating agents that can modify the N7 and O6-positions of guanine to generate chloroethyl adducts (Figure 6). Importantly, O6-chloroethyl guanine (O6Cl-ethylG) adducts undergo rapid chemical rearrangement to react with nearby cytosine bases to generate guanine–cytosine (G–C) interstrand crosslinks that are highly cytotoxic. [21]

Bifunctional alkylating agents have similar reactive properties to monofunctional alkylating agents but contain two active moieties that can react with separate bases of

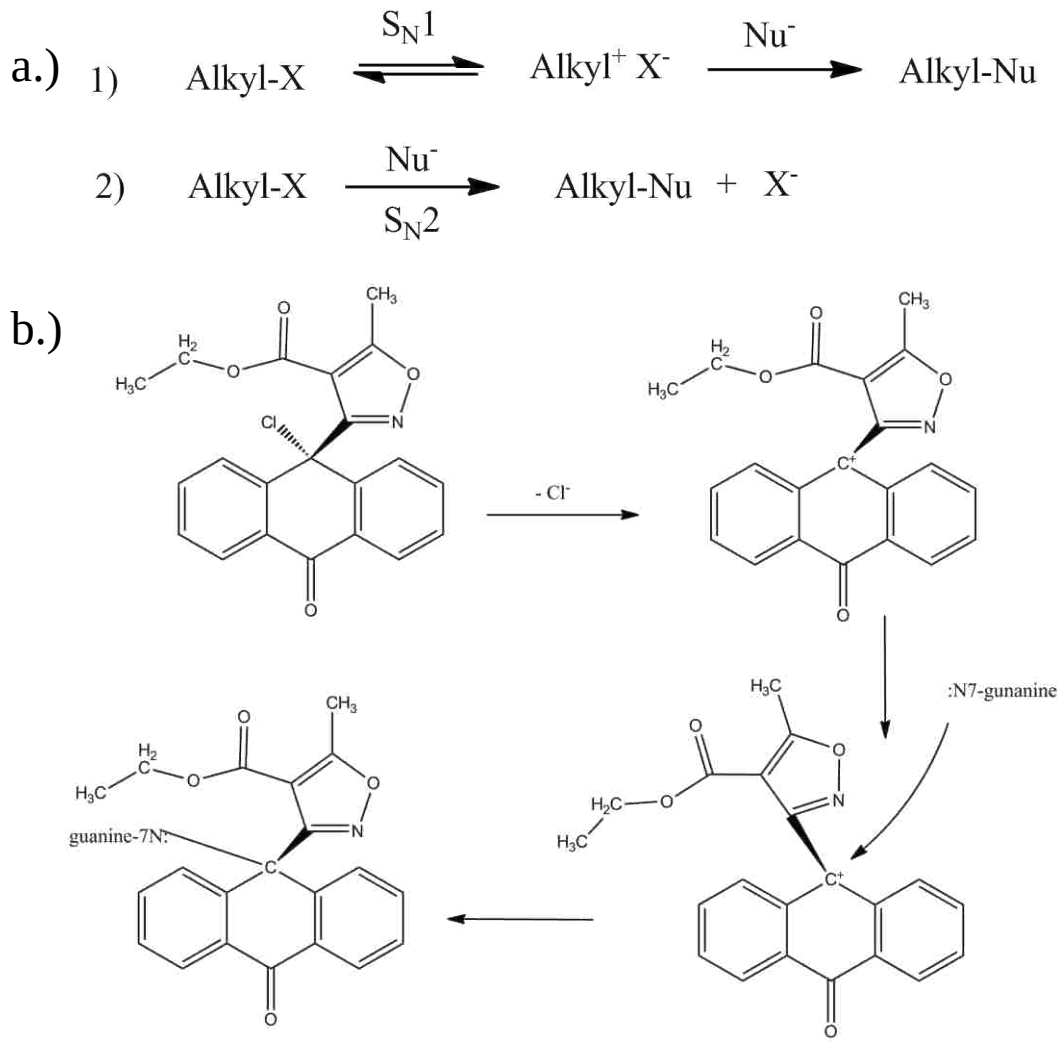

Scheme 1. Mechanisms of nucleophilic substitution. a.) Nucleophilic substitution mechanism. b.) Mechanism for alkylation of DNA

DNA to form interstrand crosslinks in addition to monoadducts (Figure 6). The nitrogen mustards and aziridine compounds are two major classes of bifunctional alkylating drugs used for cancer treatment that can crosslink DNA through an aziridinium-ring intermediate. Nitrogen mustard compounds react readily with N7-guanine and, to a lesser extent, with N3-adenine and N7-adenine to form bulky N-monoadducts. These adducts can subsequently react with another base to form guanine–guanine (G–G) and guanine–adenine (G–A) interstrand crosslinks (Figure 6).

Depending on their position in DNA, the different base adducts that are introduced by alkylating agents can compromise genome integrity by inducing mutagenesis (thereby promoting cancer induction) and/or by blocking essential biological processes such as DNA replication and transcription (which could potentially lead to cell death). Moreover, certain lesions can also be processed into clastogenic and cytotoxic products that can engage other DNA repair pathways or that can induce programmed cell death. It is important to note that other biological molecules are also subject to alkylation damage, including RNA, protein, lipids and mitochondrial DNA. Thus, a single chemotherapeutic alkylating agent can modify a variety of biological molecules to generate a range of lesions that can elicit a number of biological effects. [21]

3.1 G-quadruplex Structure

3.1.1 The G-quadruplex backbone

The fundamental unit of the G-quadruplex is the G-quartet, which is built from the association of four guanine bases in a cyclic motif (Figure 4). Utilizing both Hoogsteen hydrogen bonding and Watson–Crick faces, the tetrad is a square shaped unit stabilized by eight hydrogen bonds (N1–O6, N2–N7) with the O6 atoms pointing

centrally into the ring to form an anionic anti-prismatic bipyramidal cage (Figure 7). The planar tetrad can further associate to form extended 3D structures exploiting their large aromatic π-surfaces, which are bigger than the Watson-Crick base pairs. The square aromatic surface is then further stabilized by association of metal ions that intercalate into the central channel (Figure 7), and this difference constitutes the basis for designing G-quadruplex specific ligands.[5, 22-23]

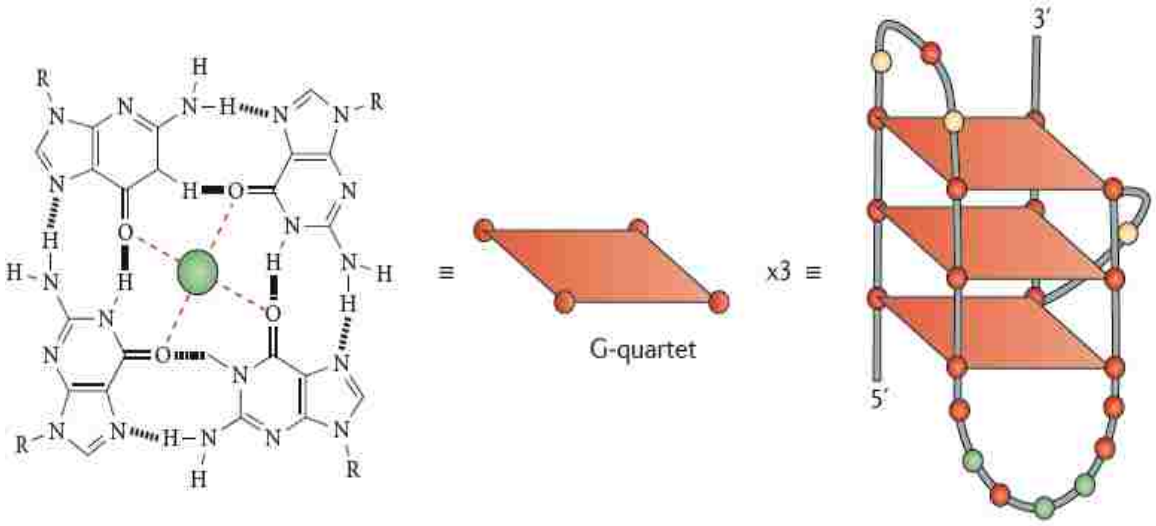

Figure 7. Guanine Base Pairing & Quadruplex Structures. Reprinted from reference [14] with permission from the publisher.

3.1.2 Topology for potential G-quadruplex binders

G-quartets can stack on top of each other to form four-stranded G-quadruplexes (Figure 7). These structures exhibit extensive structural diversity and polymorphism relative to duplex DNA. In general, structural polymorphism arises mostly from the nature of the loop, such as variations of strand stoichiometry, strand polarity, glycosidic torsion angle(s), and the location of the loops that link the guanine strand(s). Meanwhile, the solution environment, such as the presence of metal ions, ligands, or molecular

crowding conditions, may also influence the topology of quadruplex.[5] G-quadruplexes can be folded from a single G-rich sequence intra-molecularly (parallel) or by the intermolecular association of two (dimeric or bimolecular, antiparallel or parallel) or four (tetrameric or tetramolecular, parallel) separate strands.[5, 24] The telomeric G-quadruplex-forming sequence structures has been summarized by Ou et al. (see Figure 8).[5] The stacked tetrads remain planar, with a similar rise and twist and the direction (5' to 3') that the phosphodiester backbone runs can vary. In duplex DNA and RNA, an anti-parallel arrangement is required, while quadruplexes can accommodate any combination of directions, giving rise to both parallel and anti-parallel alignments[22] (Figure 9a). For example, two intramolecular G-quadruplex structures have been identified from the human telomeric sequence as the basket-type and propeller-type, depending on the incubation conditions (Figure 9).[24]

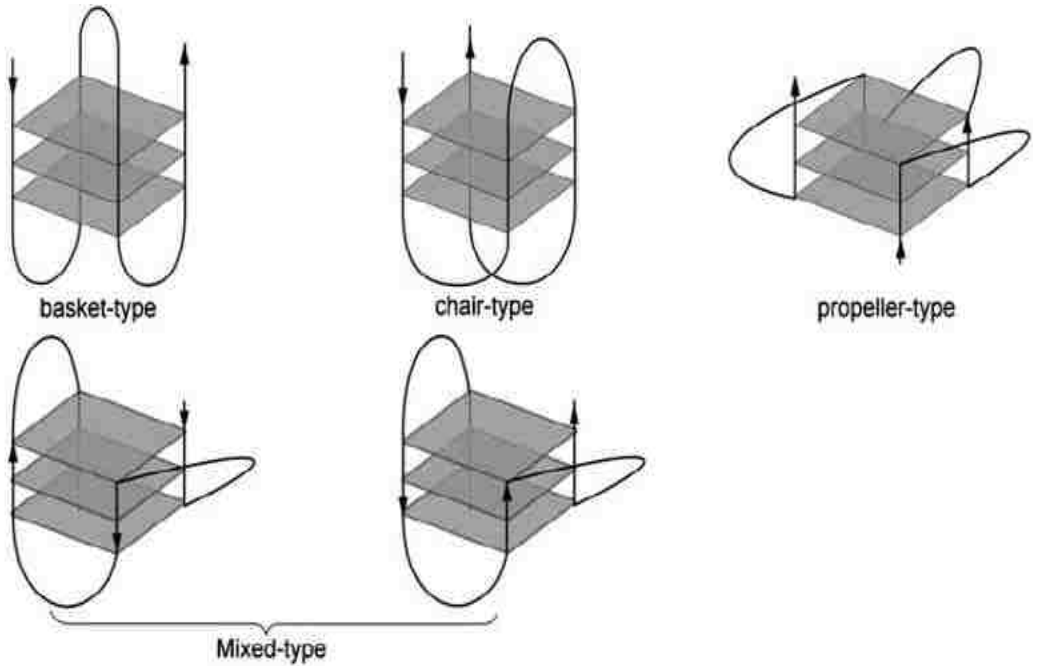

Figure 8. G4-DNA topologies and diversities. Reprinted from reference [6] with permission from the publisher.

Variations in strand polarity also affect the location of the linkers, or loops between G-rich segments. As shown in Figure 9a, parallel G-strands require a connecting loop to link the bottom G-tetrad with the top one, leading to propeller-type loops. In general, the sequence and size of the loops play an important role in determining the topology and stability of quadruplexes. In addition, loop residues can themselves form stacking and hydrogen bonding interactions, further stabilizing (or destabilizing) G-quadruplex folds, while longer linker lengths favor antiparallel backbone alignments, which may also contain guanine residues that could be expected to form part of a guanine tetrad.[5] A recent molecular dynamics simulation has revealed that the sequences of the connecting loops in quadruplexes are the major contributors to quadruplex flexibility and are the potential sites for drug binding. [5, 16-18, 22-23, 25]

The central coordinated charged cavity can accommodate a variety of metal cations of different radii that strongly influences not only the final folded topology of the stacked quadruplex but also its stability. The metal ion stabilizing influence is linked to the increasing radii from Li+ < Na+ < K+ with potassium being optimal, and dramatically increasing G-quadruplex stability. The hole between G-tetrads is well suited to coordinating cations of this size because the two planes of tetrads are lined by eight carbonyl O6 atoms (with strong negative electrostatic potential) that create a central negatively charged channel inside the G-tetrad stack (Figure 9b).[5, 16-18, 22-25]

In solution, many quadruplex-forming sequences adopt multiple folding topologies depending on the length of individual G-quartets, loop composition and size, and the type of cation. It has been reported that human genes contain as many as 376,000

quadruplex-forming sequences.[26] Databases used in screening and identifying G-quadruplex structures are very common. With the increasing number of quadruplexes

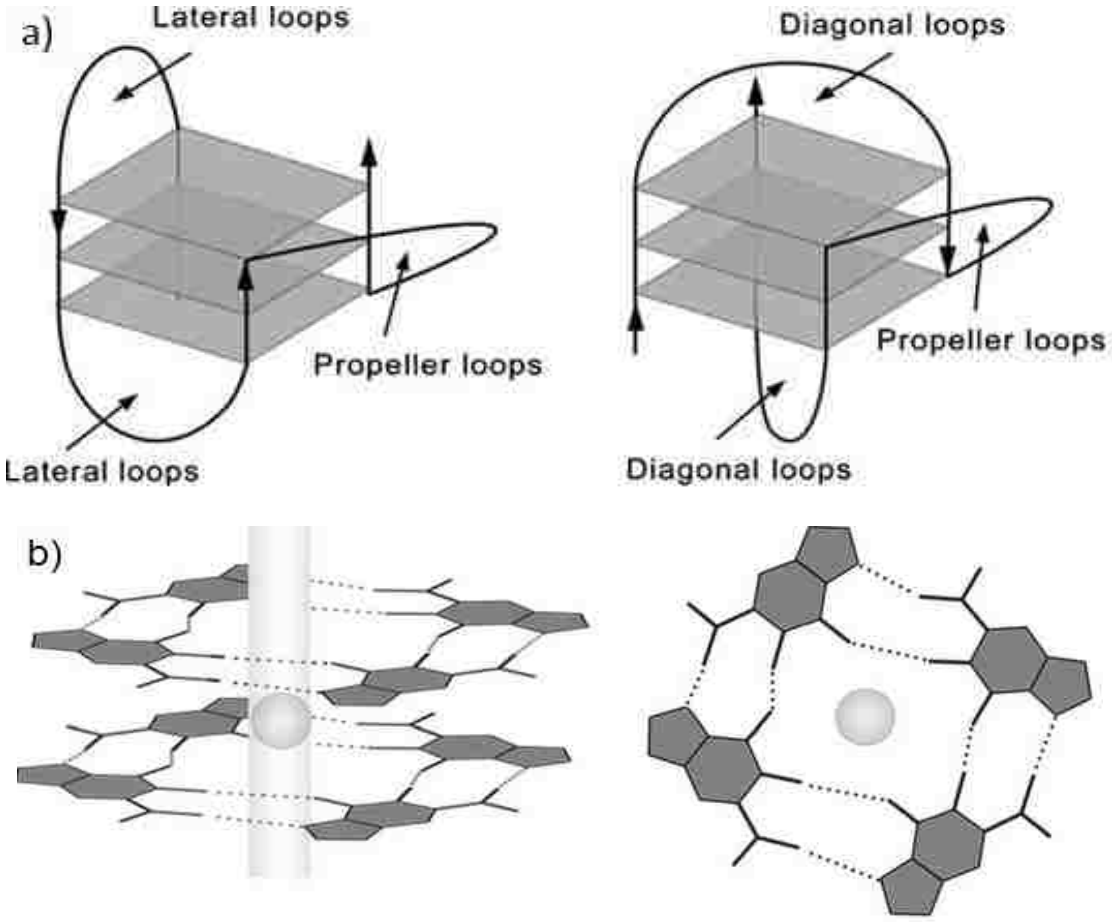

Figure 9. Basic G-Quadruplex building blocks. Reprinted from reference [6] with permission from the publisher.

reported in genomic studies, drug design must be directed not only to differentiating between duplex and quadruplex DNA species, but also to recognizing different quadruplex species. The area of G-quartets, loop regions, groove dimensions, and the negative electrostatic potential of the anionic backbone and the central channel of G-quadruplexes are critical elements that need to be considered in order to improve the binding selectivity of drug candidates.[5]

4.1 G-quadruplex Binding Ligands

4.1.1 Quadruplex DNA Small Molecule Interactions

Small molecules that induce the formation of, and/or selectively bind to, G-quadruplex structures are of interest for development as potential therapeutic agents, particularly in the anticancer therapeutic area. Of the quadruplex binding molecules identified to date, many are based on core functionalized polycyclic heteroaromatic systems such as acridines, anthraquinones, perylenes or porphyrins (Figure 10). A few of these have been shown to produce G-quadruplex-related biological effects even though their physicochemical features are conventionally non-drug-like. A common approach to G-quadruplex ligand design involves taking these relatively large aromatic ring systems as a starting-point on the basis that they can interact with the terminal G-quartets of a quadruplex through π–π interactions (end-stacking). Thus, the first small molecule reported to bind to G-quadruplex DNA was an anthraquinone derivative. Following this, molecules containing similar structural motifs such as fluorenones and acridines were described. As aromatic groups alone are insufficient to confer high binding affinity, and their hydrophobicity reduces water solubility, they have frequently been functionalized with one or more cationic side chains to improve solubility and enhance potential bonding interactions with backbone phosphates and functional groups in the unique loops and grooves found in G-quadruplex structures.[3, 27]

In addition, several G-quadruplex-targeting ligands designed to date have shape characteristics that minimize duplex DNA interaction. This design strategy is apparent in the acridine derivative BRACO-19, the first synthetic G-quadruplex ligand to have significant selectivity compared to duplex DNA. Other polycyclic G-quadruplex-binding

ligands include TMPyP4 (a cationic porphyrin), telomestatin (a cyclic oxazole-containing natural product from *Streptomyces anulatus*), and RHPS426 (a polycyclic acridine)

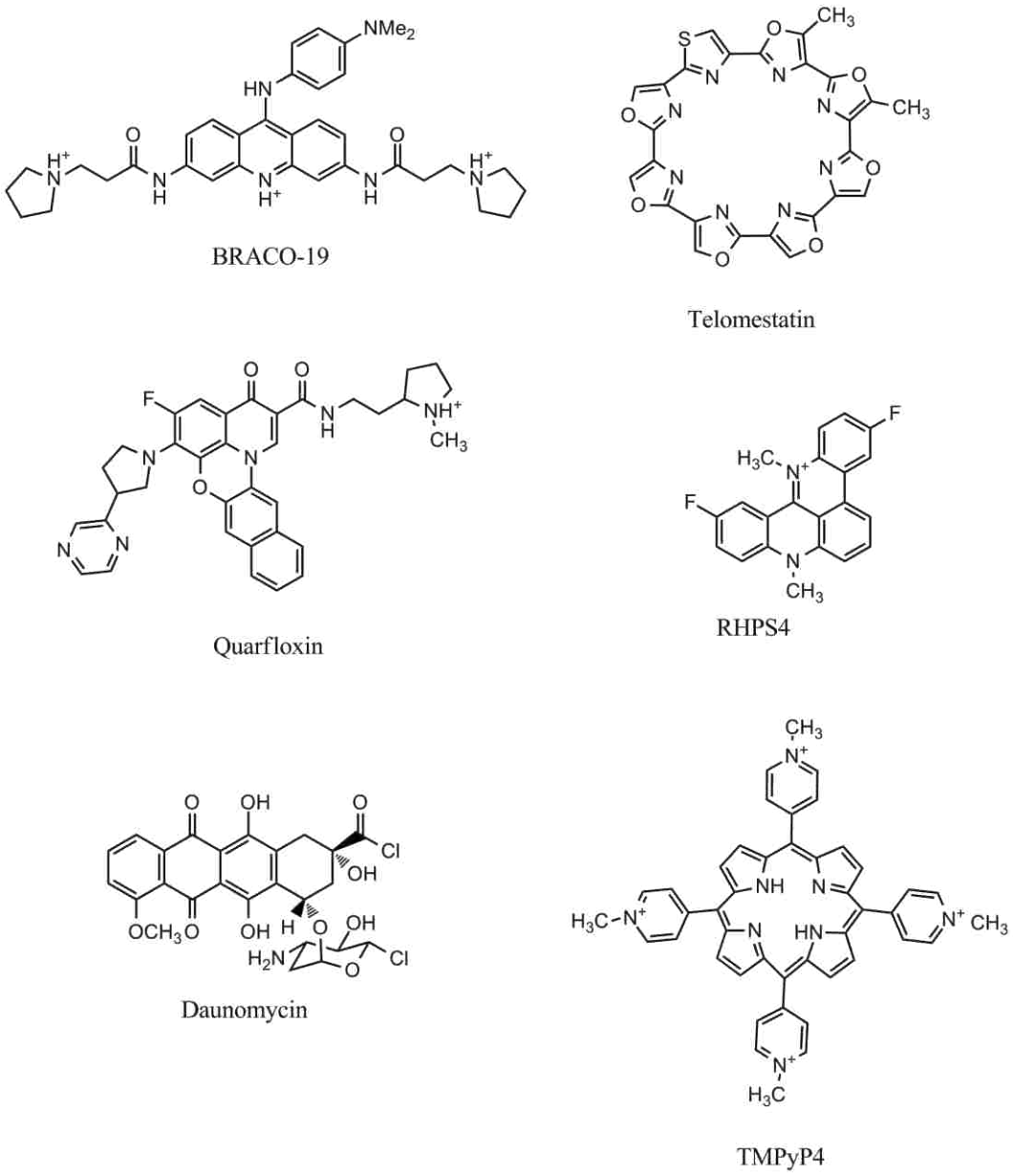

Figure 10. Quadruplex-DNA binding molecules

(Figure 6). The large planar surfaces of these compounds, their high molecular weights (600 or above) and lipophilicity, and (for some) their significant charge and poor water

solubility indicate that they are mostly non-drug-like and deviate from the Lipinski Rule of Five in terms of their potential for oral bio-availability.[3] More recent reports have demonstrated that non-conjugated compounds that are synthetically more accessible than telomestatin can have potency against telomerase and quadruplex selectivity. Many quadruplex-binding ligands have been reported subsequently, although relatively few have been evaluated in cell-based assays, or even with reliable *in vitro* telomerase assays.[4, 27] To date, quarfloxin (Figure 10) is the only G-quadruplex ligand from the large number that have been developed to have progressed to clinical evaluation.[3]

G4-DNA binding molecules have been the subject of much study in the new millennium with many examples showing a high degree of selectivity and binding stability.[28-33] However, daunomycin (Figure 10) is already a compound used in general medical practice to treat cancer and has appreciable G4-DNA binding affinity. This data suggests that the antitumor activity of daunomycin may in fact be due, in some part, to quadruplex stabilizations in genomic DNA.

It is proposed that designing the optimal G4-DNA binder must also contain some mimic of a bio-molecule (e.g. peptide bonds) so as to minimize recognition as an antigen, quick metabolism, and excretion from the body before it can exert its function. Because of the compact nature of duplex DNA a G4-DNA binding ligand would need to be pre-organized so that unfavorable steric interactions would keep the required large planar group from intercalating between the base pairs. Figure 11 illustrates the isoxazole systems, containing an anthracene or anthrone ring system with a hydrogen bond acceptor ethyl isoxazole ester, which could serve the purpose addressing all of the important factors (i.e. pre-organization, hydrogen bond acceptor/donor, and small size).

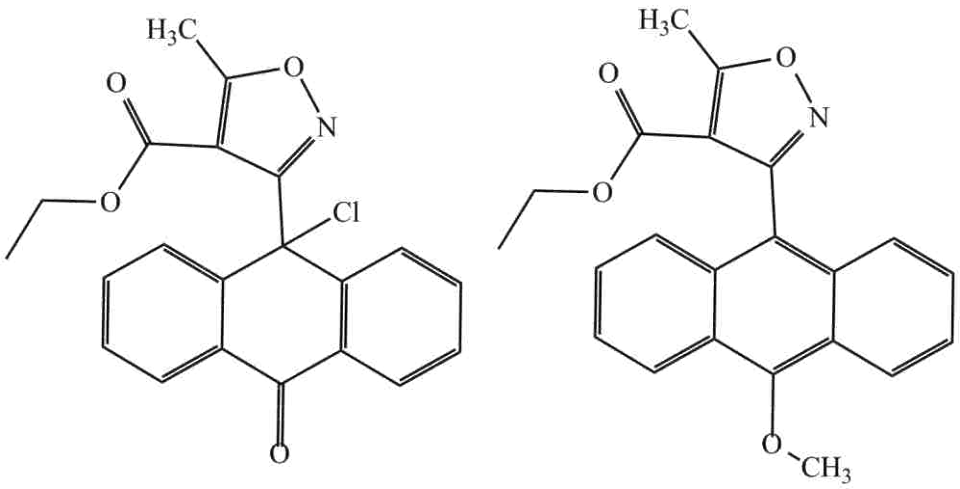

Figure 11. Combining functionalities to form a selective G4-DNA ligand.

4.1.2 Structural Features of a non-B-DNA binder

The anthracene isoxazole ester system (AIE) (Figure 11) was designed so as not to intercalate B-DNA because of the small distance between the isoxazole and anthracene moieties. AIE was designed to mimic the behavior of guanines and stabilize or induce the G-quadruplex structure, which in turn can inhibit telomerase activity. The essential pharmacophore for telomerase inhibition is a large aromatic core that favors planar π-π stacking interactions with the G-tetrads. Positively charged side chains that interact with the DNA grooves, can exploit the central electronegative channel to enhance binding. Electrostatic interactions between ligand side chains and DNA phosphates play a major role in the formation and stabilization of G-quadruplex structures and in selecting its topology; so the presence of a cationic center on side chain is favorable for optimal electrostatic interactions with negative charges on the phosphate backbone of DNA. The size of the side chain is also important, and small tether length has better inhibitory

activity. Existence of an atom which can form a hydrogen bond is favorable, especially an oxygen atom..[2]

Also, Neidle had previously shown that there were several possible binding modes (Figure 12) for amidoanthracne-9, 10-diones to quadruplex DNA based on

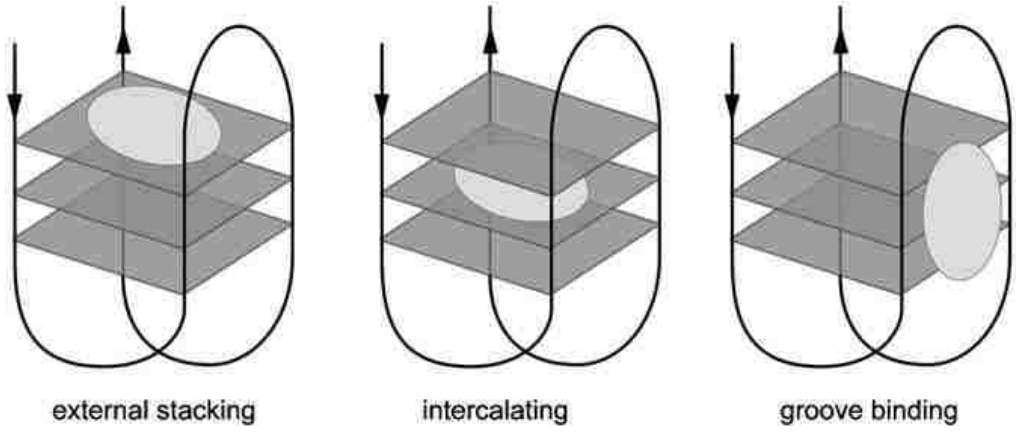

Figure 12. G-quadruplex small molecule stabilization binding modes. Reprinted from reference [54] with permission from the publisher.

substitution using molecular modeling,[33-35] stopped-flow kinetics,[36] thermal DNA melting,[35] and X-ray crystalography.[35] Hurley showed that the porphyrns 5,10,15,20-tetra-(N-methyl-2-pyridyl)porphine (TMPyP2) and 5,10,15,20-tetra-(N-methyl-2-pyridyl)porphine (TMPyP4) (Figure 10), bind G-quadruplex structures externally atop the G-tetrad.[37] Furthermore, Hurley and Neidle described in a review how quindoline and Berberine (related plant alkaloid) are classic G-quadruplex binding agents with their derivatives showing significant anti-proliferative properties in cancer cell lines; as well as, the two current standards in quadruplex binding: telomestatin and tri-substituted isoalloxazines.[14] Given these findings we felt the next step was to use computer based molecular modeling to determine which mode of binding best suited the AIE system.

5.1 10-Methoxy anthracene isoxazole ester synthesis

Scheme 1 outlines the modified synthesis method from the oxime used by Natale and coworkers [38-40] to generate anthracene isoxazole ester **1**. Initial bromination of **2** was successful in methylene chloride with a slight modification from Cakmak and coworkers[41]. Subsequent methylation of **3** was achieved with the addition of a 1.2-fold excess of sodium methoxide *in situ* in warm DMF yielding **4** in good yields.

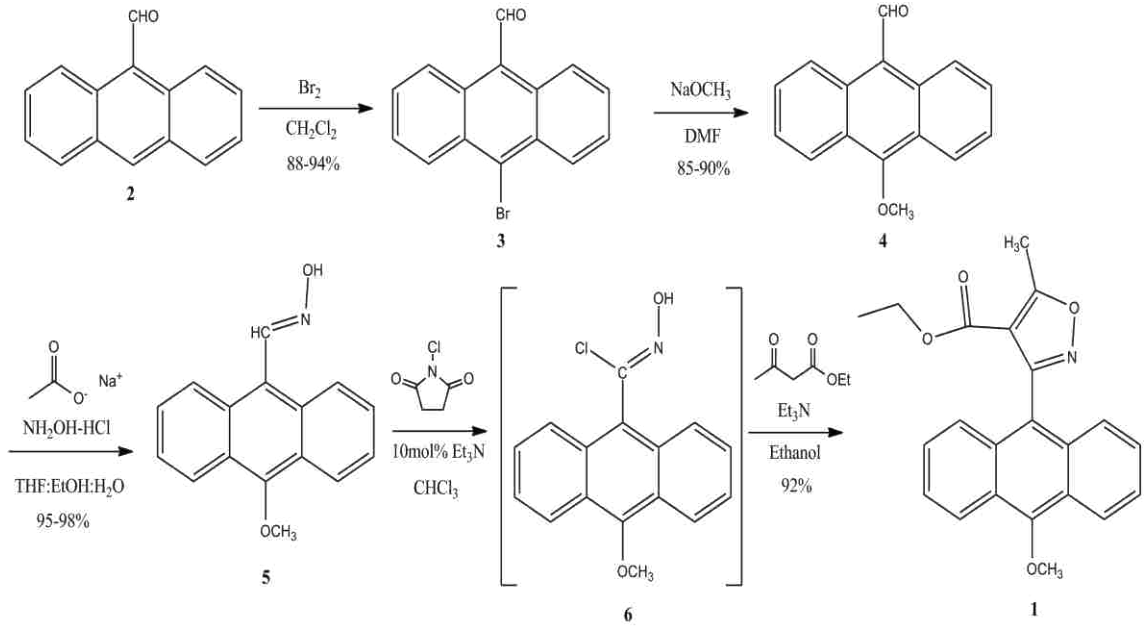

Scheme 2. Method for the formation of anthracene isoxazole ester 1

Oxime formation from the aldehyde of **4** with hydroxyl amine hydrochloride and sodium acetate in refluxing DMF afforded the oxime **5**. Formation of the oximinoyl chloride intermediate **6** was performed using recrystallized N-Chlorosuccinamide (from benzene) and $CHCl_3$ at room temperature (yield not calculated). Finally, **6** was reacted with triethylamine and ethyl acetoacetate in absolute ethanol to give the final product **1** in 92% yield after two steps.

6.1 Anthrone isoxazole ester

Scheme 2 outlines the anthrone synthesis combined with the method used by Natale and coworkers[40] to generate symmetrical anthrone isoxazole ester **13**. Subsequent oxime formation from the aldehyde **8** was achieved with the addition of a 2.0 eq. excess hydroxylamine hydrochloride and a 3.5 eq. excess of sodium acetate in THF:EtOH:H_2O until the no slurry was observed yielding **9**.

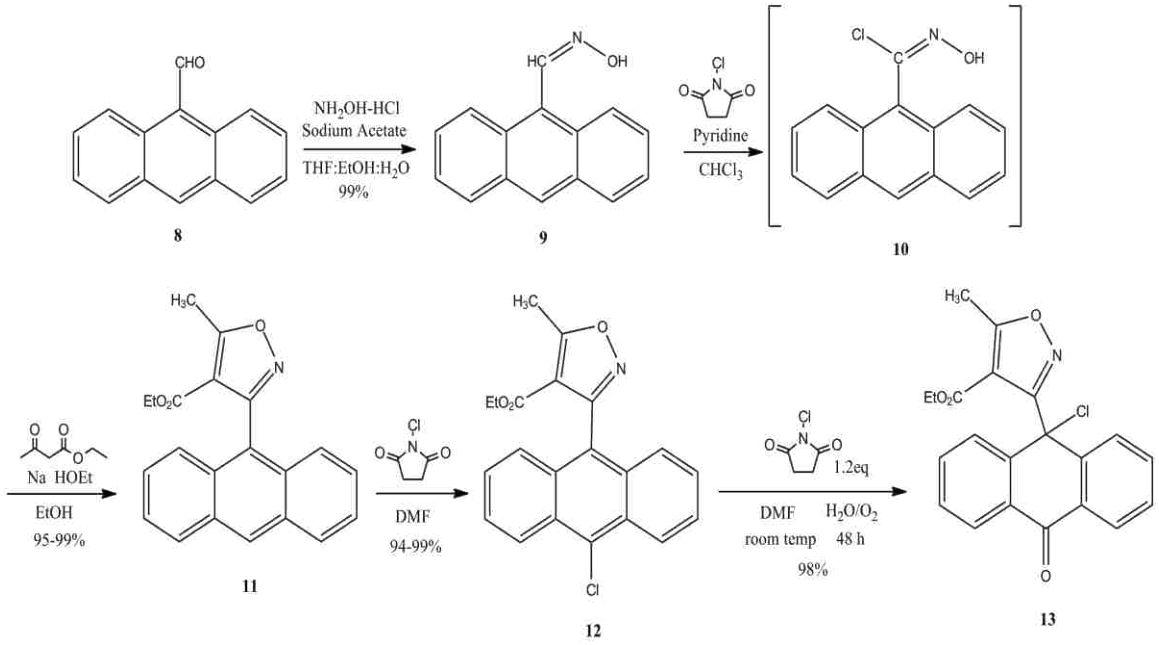

Scheme 3. Method for the formation of anthrone isoxazole ester 13

Formation of the oximinoyl chloride intermediate **10** was performed using recrystallized N-Chlorosuccinamide (from benzene) and dry $CHCl_3$ at 45^oC (yield not calculated). Oximidoyl chloride **10** was reacted with sodium ethoxide and ethyl acetoacetate in absolute ethanol to give the product **11** in great yields after two steps. The subsequent chlorination of **11** was achieved with a slight modification from the procedure of Natale and coworkers[40]. Finally, another chlorination reaction with NCS in DMF gave the final product **13**.

The regiochemistry of the final product **13** was determined by 2D correlation spectroscopy or HSQC (Heteronuclear Single Quantum Coherence). **Figure 13** illustrates an example of how the proton assignments and regiochemistry were made from a HSQC experiment of anthrone product **13**. The numerical labels such as 8.31, 182.5, and 0.05 indicate protons correlated, carbons correlated and intensity. The peri-aryl protons H-9 & H-19 are easily spotted at ppm 7.26 by their strong J2 coupling and chemical shift which have a strong correlation to the tertiary carbon at ppm 62. It is clear that H-12 and H-16 are down field at ppm 8.31 correlating to the carbonyl carbon ppm 182.

7.1 Anthrone isoxazole ester crystal structure

The crystal structure of ethyl 3-(9-chloro-10-oxo-9, 10-dihydroanthracen-9-yl)-5-methylisoxazole-4-carboxylate (**13**) was obtained. It possesses similar bond lengths and angles as the previously reported isoxazole ester, ethyl 3-(10'-chloro-9'-anthracenyl)-5-methyl-4-isoxazolecarboxylate. The anthrone is virtually planar, and adopts a shallow boat conformation, as evidenced by the absolute sum of the six intra- B-ring dihedral angles (40.9081°). The compound adopts a conformation wherein the isoxazole ring is roughly orthogonal (torsion angle: C60 C56 C62 C63, 67.0°) to the anthrone ring (see Figure 14) with the isoxazolyl ester carbonyl O(7) being located within 3.3Å of the anthrone carbon C(31). Furthermore, in the unit cell the anthrone H(6) of one molecule of the title compound is within 3.3Å of C(22) of the second molecule at a dihedral angle of ~30^{o}, consistent with an edge-to-face π-stacking interaction. This conformation could be a vital factor in the study of the binding of this species in the drug-DNA complex in further research.

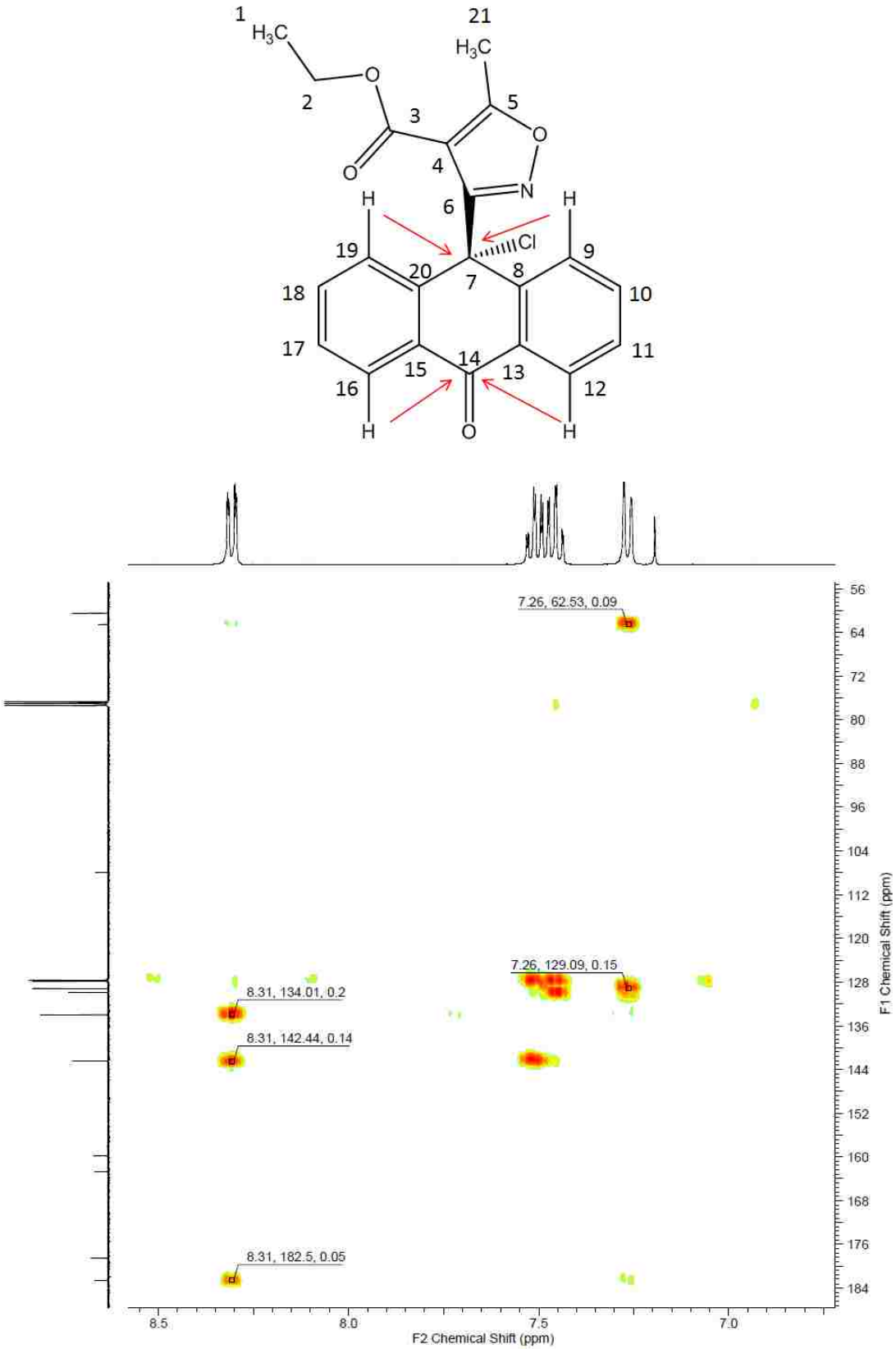

Figure 13: HSQC of **13**, shows proton shift, carbon shift, and correlation intensity.

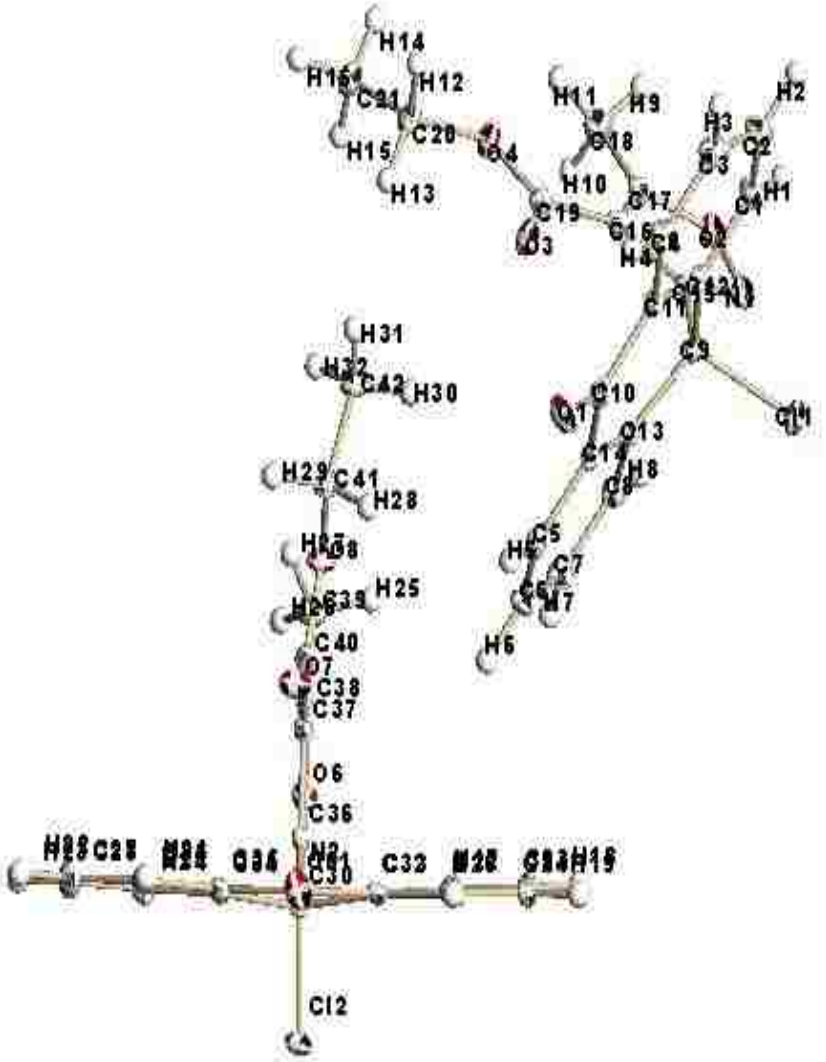

Figure 14: ORTEP diagram of **13**.

8.1 Experimental Section

All starting chemicals were purchased from Aldrich Chemical Company and used without any further purification unless otherwise indicated. Solvents were reagents grade and dried just prior to use by standard methods. Melting points were determined in open capillary tubes on a Melt-Temp apparatus and are uncorrected. High resolution mass spectra (HRMS) were obtained using a Micromass electrospray ionization (ESI)/time-of-flight mass spectrometry (LCTOF). NMR spectra for preliminary identification of products were collected on a Bruker AC200 (UltraShield™ 400MHz) using X-Win NMR (3.1). Mass spectrometer samples were introduced using a Waters model 2690 separations module HPLC fitted with a C-18 reversed phase column (2.1 mm i.d., 5 cm). Flash chromatography was performed using Sorbent Technologies standard silica gel (60 Å) with reagent grade solvents using in house compressed air.

8.1.1 Method of 10-methoxy anthracene isoxazole ester formation

To a suspension of **2** (4.175g, 20.244mmol; Sigma-Aldrich, 97%) in methylene chloride (120mL) was added Br_2 (1.1 eq., 1.2mL, 23.428mmol) diluted in methylene chloride (5mL) drop wise over 5 minutes. The reaction was covered with septa and guard column (charged with $CaCl_2$ and NaOH(s)) and allowed to stir at 63°C until TLC showed no starting material remained (ca. 5 hours). Once the solution reached room temperature, 25g Na_2SO_3 in 200mL H_2O was added to neutralize excess Br_2. The solution was then transferred to a separatory funnel, washed with 50mL metheylene chloride and the organic layer extracted and dried with sodium sulfate and concentrated under reduced pressure to yield **3** (Rf=0.34, 10:1 Hex/EtOAc, Figure 15). Recrystallized from chloroform/hexanes.

10-Bromoanthracene-9-carbaldehyde (3). (83%) ^{1}H NMR($CDCl_3$) δ 11.52 (s, 1H), 8.90-8.93 (m, 2H), 8.69-8.71 (m, 2H), 7.64-7.74 (m, 4H). ^{13}C NMR ($CDCl_3$) δ 193.28, 131.94, 131.82, 130.29, 129.02, 128.91, 128.29, 128.29, 127.47, 127.40, 125.70, 123.84. mp 205-208°C. Spectral data are in accord with those reported previously.[42-43]

The brominated aldehyde **3** (0.150g, 0.5261mmol) was taken up in 2mL of DMF (dried over sieves) under a nitrogen atmosphere. Freshly distilled methanol (1.2 eq., 0.03mL) was added via syringe. Sodium hydride (1.2 eq., 0.0253g) was added with a water condenser. The solution was allowed to stir at 60°C for 3.5 hours under an argon atmosphere. Once the solution cooled to room temperature, 50mL DI H_2O and 50mL diethyl ether was added and allowed to stir for 15 minutes. The solution was transferred to a separatory funnel and washed with 50mL diethyl ether. The combined organic layers were washed with 50mL Brine, dried over sodium sulfate and concentrated under reduced pressure. The solid was taken up in minimal methylene chloride and ran on a prepared hexanes silica column in 12:1 (Hexanes:EtOAc) until all desired product **4** was collected (Figure 16).

10-Methoxyanthracene-9-carbaldehyde (4). (85%) ^{1}H NMR ($CDCl_3$) δ 11.49 (s, 1H), 9.09 (d, J=9.03, 2H), 8.42 (d, J=8.66 Hz, 2H), 7.70-7.74 (m, 2H), 7.58-7.62 (m, 2H), 4.22 (s, 3H). ^{13}C NMR ($CDCl_3$) δ 191.93, 159.18, 134.12, 133.89, 129.34, 127.23, 125.60, 124.21, 123.96, 123.11, 121.17, 63.96. MS (EI) *m/z* 236 (22.37, M+), 237(100, M+1), 238 (18.80, M+2). (Rf=0.46 4:1:1 Hex/EtOAc/DCM).

To a suspension of **4** (0.1659g, 0.6302mmol) in 200 proof ethanol (23mL) was dissolved hydroxylamine hydrochloride (2.5eq, 0.1095g, 1.58mmol) and pyridine (20eq, 1mL, 12.4mmol) The reaction was covered with a septa and water condenser and let

reflux (ca. 80°C) for 2 days under an argon atmosphere. The solution was first concentrated under reduced pressure then transferred to a separatory funnel and washed 1 x 50mL 1N HCl (cold) and the combined aqueous layers washed 2 x 20mL CH_2Cl_2, dried over sodium sulfate, filtered, and the solvent removed under vacuum. The solid was then chromatographed on a prepared hexanes silica column starting with 8:1:1 Hex/EtOAc/DCM, 4:1:1, and finally 2:1:1 until desired product **5** was all collected (Figure 17).

10-Methoxyanthracene-9-carbaldehyde oxime (5): (79%) ^{1}H NMR ($CDCl_3$) δ 9.20 (s, 1H), 8.45-8.46 (m, 2H), 8.36-8.38 (m, 2H), 7.53-7.60 (m, 4H), 4.17 (s, 3H). ^{13}C NMR ($CDCl_3$) δ 154.22, 148.95, 131.20, 126.90, 125.36, 125.29, 124.29, 122.72, 119.83, 63.45. MS (EI) *m/z* 234 (100, M-H_2O), 235 (28.54, M-$H_2O)^+$, 252 (38.87, M+1). (Rf=0.34, 4:1:1 Hex/EtOAc/DCM).

The starting oxime **5** (0.0905g, 0.3601mmol) was taken up in 10mL of chloroform at room temperature, to which the solution was added Et_3N (1.23eq, 0.045g) and recrystallized NCS (1.45eq, 0.0697g, .52198mmol) over 5 minutes. The solution was allowed to stir at room temperature under argon for 2 hours. The organic layer was washed with 1 x 100mL DI H_2O, then the aqueous layer washed 1 x 20mL $CHCl_3$, dried with sodium sulfate, filtered, and the solvent removed under reduced pressure to yield **6**. The intermediate **6** was purified only through extractive isolation using water and $CHCl_3$ and taken on to the next reaction as is. To a solution of **6** in absolute ethanol (20mL) was added 1.75 equivalents of ethyl acetoacetate (0.0741g, 0.6314mmol) and 1.91eq. Et_3N (0.0696g, 0.6878mmol). The mixture was allowed to stir at 40°C under argon for 30 hours until TLC in 4:1:1 Hex/EtOAc/DCM revealed all nitrile oxide had been consumed.

Finally, the ethanol was removed via rotary evaporation and the solid dissolved in $CHCl_3$, washed 2 x 50mL Brine, and the aqueous layer washed 1 x 20mL $CHCl_3$, dried sodium sulfate, and concentrated under reduced pressure. The solid was then chromatographed using 1:1 Hex/EtOAc, then 1:2 and flushed with EtOAc until all desired product **1** (Figure 18) was collected.

N-hydroxy-10-methoxyanthracene-9-carbimidoyl chloride (6): Was not purified, carried on through *in situ* procedure only. ^{1}H NMR(400 MHz, $CDCl_3$) δ 8.36 (d, J=8.78 Hz, 2H), 8.31 (d, J=8.78, 2H), 7.70 (t, J=15.06, 7.40 Hz, 2H), 7.60 (t, J=15.31, 8.28 Hz, 2H), 4.20 (s, 3H).

Ethyl 3-(10-methoxyanthracen-9-yl)-5-methylisoxazole-4-carboxylate (1). 32%. (Rf=0.17 1:2 Hex/DCM, Rf=0.49 4:1:1 Hex/EtOAc/DCM). ^{1}H NMR(400 MHz, $CDCl_3$) δ 8.37 (d, J=8.77 Hz, 2H), 7.65 (d, J=8.53 Hz, 2H), 7.51 (t, 2H), 7.43 (t, 2H), 4.20 (s, 3H), 3.71 (q, J=7.15 Hz, 2H), 2.93 (s, 3H), 0.35 (t, J=7.15 Hz, 3H).

8.1.2 Method of anthrone isoxazole ester formation

To a suspension of **8** (4.0g, 19.39mmol; Sigma-Aldrich, 97%) in THF: Ethanol: H_2O (54mL: 27mL: 27mL) was dissolved sodium acetate (3.5 eq., 5.57 g, 67.89mmol) and hydroxylamine hydrochloride (2eq, 2.69g, 38.71mmol). The reaction was covered with a septa and let stir at room temperature until TLC showed no starting material remained (ca. 49 hours). The solution was then transferred to a separatory funnel and washed 4 x 200mL Brine and the combined aqueous layers washed 2 x 50mL $CHCl_3$, dried over sodium sulfate, filtered, and the solvent removed under vacuum to yield **9** **(**Figure 19).

Anthracene-9-carbaldehyde oxime (9). 99%. (Rf=0.53 4:1:1 Hex/EtOAc/DCM), ^{1}H NMR ($CDCl_3$) δ 9.22 (s, 1H), 8.51 (s, 1H), 8.42 (d, J=8.66 Hz, 2H), 8.03 (d, J=8.16 Hz, 2H), 7.50-7.59 (m, 4H). ^{13}C NMR ($CDCl_3$) δ 148.98, 131.30, 130.21, 129.35, 128.86, 128.81, 126.78, 126.42, 125.39, 124.97, 123.64.

The starting oxime **9** (4.667g, 21.09mmol) was taken up in 120mL of chloroform at room temperature, to which a solution of pyridine (10mol%, 2.00mL) and recrystallized NCS (1.1eq, 3.098g, 23.20mmol). The solution brought to 45ºC for 3.5 hours then cooled to room temperature. The organic layer was washed with 4 x 200mL Brine and 2 x 150mL H_2O, then the aqueous layer washed 2 x 150mL $CHCl_3$, dried with sodium sulfate, filtered, and the solvent removed under reduced pressure to yield **10**. The intermediate was purified only through extractive isolation using brine and $CHCl_3$ and taken on to the next reaction as is. To a solution of **10** in absolute ethanol (100mL) was added 1.4 equivalents of ethyl acetoacetate (3.8425g, 29.53mmol). In a separate round bottom was added 50mL absolute ethanol and 1.018g Na(s). Once the sodium dissociation had completed, the warm solution was added to the nitrile oxide and the mixture was allowed to stir at room temperature under argon for 21.5 hours until TLC in 4:1 Hex/EtOAc revealed all **10** had been consumed. Finally, the ethanol was removed via rotary evaporation and the solid dissolved in $CHCl_3$, washed 4 x 200mL Brine, and the aqueous layer washed 2 x 150mL $CHCl_3$, dried sodium sulfate, and concentrated under reduced pressure. The solid was then chromatographed using 4:1 Hex/EtOAc to give desired product **11** (Figure 20).

N-hydroxyanthracene-9-carbimidoyl chloride (10): Was not purified, carried on through *in situ* procedure only

Ethyl 3-(anthracen-9-yl)-5-methylisoxazole-4-carboxylate (11). 93%.^{1}H NMR (400 MHz, $CDCl_3$) δ 8.59 (s, 1H), 8.06 (d, J=7.91, 2H), 7.66 (d, J=8.16 Hz, 2H), 7.41-7.50 (m, 4H), 3.70 (q, J=7.15 Hz, 2H), 2.93 (s, 3H), 0.33 (t, J=7.15 Hz, 3H). ^{13}C NMR ($CDCl_3$) δ 176.16, 161.52, 160.44, 131.01, 130.82, 128.64, 128.45, 126.25, 125.44, 125.21, 122.75, 111.37, 60.02, 13.41, 12.80. Spectral data are in accord with those reported previously[38-39].

Compound **11** (0.300g, 0.905mmol) was taken up in 10mL DMF to which was added a solution over 10 minutes of N-Chlorosuccinimide (NCS) (1.2eq, 0.1461g, 1.094mmol) dissolved in 5mL DMF. The solution was brought to 43ºC and let stir for 4 hours whereupon the solution was poured into 50mL ice/water which was allowed to stir for 1 hour with the product **12** (Figure 21) precipitating out. Product was filtered and washed with 2 x 25mL DI water.

Ethyl 3-(10-chloroanthracen-9-yl)-5-methylisoxazole-4-carboxylate (12). 96%.^{1}H NMR (400 MHz, $CDCl_3$) δ 8.59 (d, J=8.91 Hz, 2H), 7.59-7.66 (m, 4H), 7.46-7.50 (m, 2H), 3.72 (q, J=7.15 Hz, 2H), 2.93 (s, 3H), 0.39 (t, J=7.15 Hz, 3H). ^{13}C NMR ($CDCl_3$) δ 176.29, 161.28, 160.15, 131.13, 131.00, 128.30, 126.67, 126.52, 125.84, 125.04, 122.60, 111.43, 60.15, 13.43, 12.91. Spectral data are in accord with those reported previously[38].

The chlorinated anthracene **12** (0.3312g, 0.905mmol) was taken up in 5mL DMF to which was added a solution over 10 minutes of N-Chlorosuccinimide (NCS) (1.2eq, 0.1451g, 1.087mmol) dissolved in 5mL DMF. The solution was brought to 30ºC and let stir for 43 hours whereupon the solution was poured into 50mL ice/water which was allowed to stir for 1.5 hours with the product precipitated out. Product was filtered and washed with DI water. The solid was dissolved in minimal CH_2Cl_2 and placed on a wet

silica column prepared with hexanes. The solvent polarity increased using a stepwise elution of 10:1, 6:1, and finally 4:1 until all **13** (Figure 22) was collected.

Ethyl 3-(9-chloro-10-oxo-9,10-dihydroanthracen-9-yl)-5-methylisoxazole-4-carboxylate (13). 29%, (Rf=0.28, 4:1 Hex/EtOAc), ^{1}H NMR($CDCl_3$) δ 8.38 (dd, J=1.38, 7.65 Hz, 2H), 7.51-7.61 (m, 4H), 7.34 (dd, J=1.13, 7.91 Hz, 2H), 3.56 (q, J=7.15 Hz, 2H), 2.70 (s, 3H), 0.65 (t, J=7.03 Hz, 3H); ^{13}C NMR($CDCl_3$) δ 182.58, 178.50,162.69, 159.76, 142.41, 133.92, 129.85, 129.13, 127.84, 127.58, 107.92, 62.51, 60.43, 13.78, 13.47. MS (EI) *m/z* 346(100, M-Cl), 347(28.33, M-Cl)$^{+}$, 348(8.42, M-Cl)$^{+2}$.

9.1 Future Direction

Many high affinity ligands have been synthesized and studied in previous reports but it is proving elusive to structurally determine ligand interactions in a routine manner. Currently the application of crystallographic techniques is providing us with the most comprehensive picture of ligand binding interactions; however the validity of the model is in some ways compromised by crystal packing forces within a crystalline lattice. Even within these constraints, it is clear that the stacked G-quadruplex core remains intact with little scope for the intercalation of planar ligands. The diverse ranges of G-quadruplex forming sequences identified and characterized appear to be very diverse, folding almost exclusively as parallel stranded motifs, thereby limiting the diversity required for selective targeting. However, although restricted in topology, the G-quadruplex forming sequences will still contain sequence variability in connecting loops, thus providing new interaction surfaces and unexpected platforms for interaction. As always, there will be a need for current (and newly discovered) G-quadruplexes to be validated in terms of

structure and (more importantly) biological role, before effort is applied to finding suitable therapeutic agents.

While Absorption, Distribution, Metabolism, Excretion, and Toxicity (ADME-Tox) is a very important part of medicine design the desired biological target should be of primary concern when considering design and this has been seriously addressed in the design of the AIE series. However, possibly one of the most important points in designing a small molecule drug is the chirality of the target biomolecule or system. The

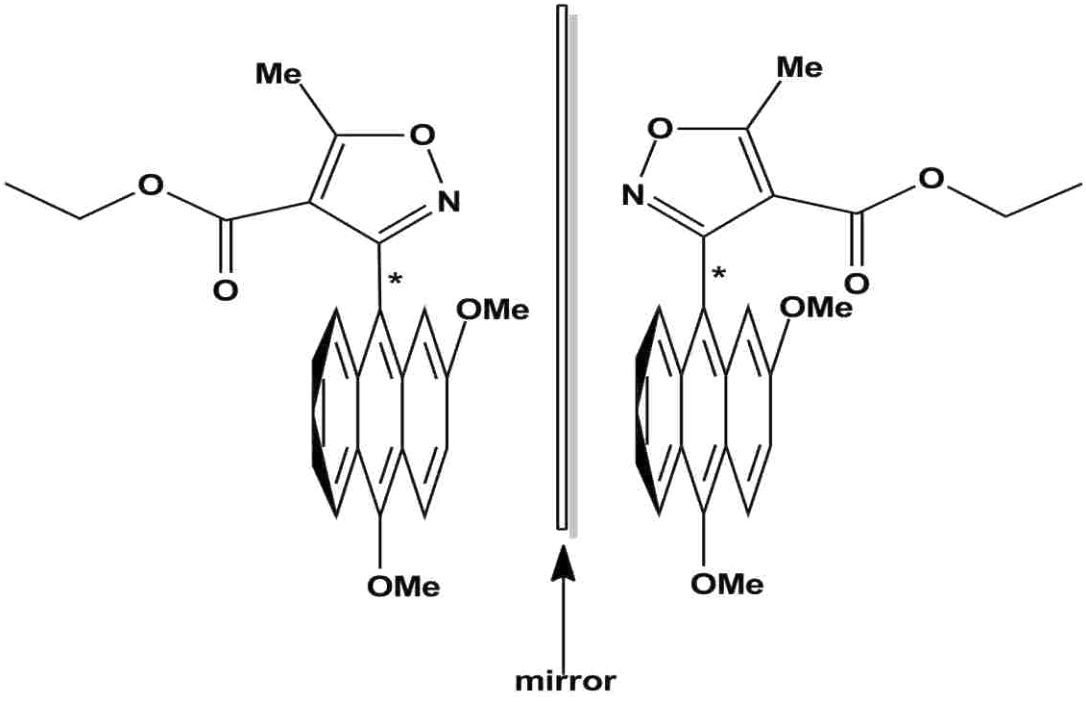

Figure 15. Axial Chiral Anthracene Isoxazole Ester

idea of using chiral small molecules for the treatment of mammalian diseases is not new, however, in the case of cancer chemotherapeutics chirality has only recently gained some consideration.[44-45] Chaires and coworkers demonstrated that (+) and (-) enantiomers of daunorubicin, for which the (+) enantiomer is a known and potent anti-tumor agent

currently used in general medical practice, selectively bind to different forms of DNA, B-DNA (Right handed helical) and Z-DNA (Left handed helical) respectively.[46] The inherent chirality of duplex DNA, RNA, and protein α-helices makes these biological structures ideal targets for chiral small molecules ligands that bind selectively. Quadruplex DNA structures are right handed helical therefore an antitumor molecule that would bind selectively to this system must possess the correct element of chirality.

It is proposed that adding an axis of chirality to one of the active compounds in the AIE series would produce an atropoisomer that should have selectivity for right or left handed helical DNA based on Chaires findings. In addition, functionalization of the anthracene, which has some related human toxicity, to somewhat resemble the major metabolite of anthracene would provide for better bioavailability and decrease the molecule's potentially toxic character (Figure 15). Though the new system may fall outside of the Lipinski range it has been shown that the AIE series is also highly active and therefore the methyl pyrrole can be removed to test the Lipinski prediction. The outcome of such a comprehensive study of functionality, ADME-Tox, and Chirality for this AIE series of compounds, as they pertain maximum efficacy in tumor cell suppression and biomolecule selectivity could be a novel class of antitumor agents that have little or no side effects. The isoxazole functionality establishes not only a pre-organized system for SAR exploration it is the biological handle that is the foundation of many medicines used in general medical practice today, and therefore should be a potent contender in the pool of small molecule antitumor agents.

References:

1) Neidle, S. Methods for studying quadruplexes: Sequence, structure, recognition and biological behavior. *Methods*. **2012**, *57*, 1-2.

2) Haider, S.M.; Neidle, S.; Parkinson, G.N. A structural analysis of G-quadruplex/ligand interactions. *Biochemie*. **2011**, *93*, 1239-1251.

3) Rahman, K.M.; Tizkova, K.; Reszka, A.P.; Neidle, S.; Thurston, D.E. Identification of novel telomeric G-quadruplex-targeting chemical scaffolds through screening of three NCI libraries. *Bioorg. Med. Chem. Lett.* **2012**, *22*, 3006-3010.

4) Neidle, S. Human telomeric G-quadruplex: The current status of telomeric G-quadruplexes as therapeutic targets in human cancer. *FEBS Journal*. **2010**, *277*, 1118–1125.

5) Kim, N.W.; Piatyszek, M. A.; Prowse, K. R.; Harley, C. B.; West, M. D.; Ho, L. C.; Coviello, G. M.; Wright, W. E.; Weinrich, S. L.; Shay, J. W. Specific Associtation of Human Telomerase Activity With Immortal Cells and Cancer. *Science.* **1994**, *266*, 2011-2015.

6) Ou, T., Lu, Y., Tan, J., Huang, Z., Wong, K., Gu, L. G-Quadruplexes: Targets in Anticancer Drug Design. *ChemMedChem*. **2008**, *3*, 690-713.

7) Watson, J. D. Origin of Concatemeric T7 DNA**.** *Nature New Biology*. **1972**, *239*, 197-201.

8) Grieder, C. W.; Blackburn, E. H. The Teleomer Terminal Transferase of Tetrahymena Is a Ribonucleoprotein Enzyme with Two Kinds of Primer Specificity. *Cell*. **1987**, *51*, 887-898.

9) a) Franklin, R. E.; Gosling, R. G. Molecular Configuration of Sodium

Thymonucleate. *Nature.* **1953**, *171*, 740-741. b) Watson, J. D.; Crick, F. H. C. A Structure of Neucleic Acids. *Nature*. **1953**, *171*, 737-738. c) Wilkins, M. H. F.; Stokes, A. R.; Wilson, H. R. Molecular Structure of Deoxypentose Nucleic Acids. *Nature.* **1953**, *171*, 138-140.

10) Cech, T. R. G-Strings at Chromosome Ends. *Nature.* **1988**, *332*, 777-778.

11) Zahler, A. M., Williamson, J. R., Cech, T. R.; Prescott, D. M. Inhibition of Telomerase by G-quartet DNA structures. *Nature*. **1991**, *350*, 718-720.

12) Harrington, L.; Zhou, W.; McPhail, T.; Oulton, R.; Yeung, D. S. K.; Mar, V.; Bass, M. B.; Robinson, M. O. Human Telomerase Contains Evolutionary Conserved Catalytic and Structural Subunits. *Genes Dev.* **1997**, *11*, 3109-3115.

13) Siddiqui-Jain, A.; Grand, C. L.; Bearss, D. J.; Hurley, L. H. Direct Evidence for a G-quadruplex in a Promoter Region and its Targeting With a Small Molecule to Repress c-MYC Transcription. *Proc. Nat. Acad. Sci.* **2002**, *99*, 11593-11598.

14) Balasubramanian, S.; Hurley, L.H.; Neidle, S. Targeting G-quadruplexes in gene promoters: a novel anticancer strategy? *Nat. Rev. Drug Discovery.* **2011**, *10*, 261-275.

15) Hurley, L. H. DNA and Associated Targets for Drug Design. *J. Med. Chem.* **1989**, *32*, 2027-2033.

16) Wang, Y.; Patel, D. J. Guanine Residues in d(T_2AG_3) and d(T_2G_4) Form Parallel-Stranded Potassium Cation Stabilized G-Quadruplexes with Anti Glycosidic Torsion Angles in Solution. *Biochemistry.* **1992**, *31*, 8112-8119.

17) Castasi, P.; Chen, X.; Moyzis, R.; Bradbury, E.; Gupta, G. Structure-Function Correlations in The Insulin-Linked Polymorphic Region. *J. Mol.*

Biol. **1996**, *264*, 534-545.

18) Simonsson, T.; Pecinka, P.; Kubista, M. DNA Tetraplex Formation in The Control Region of c-myc. *Nucleic Acids Res.* **1998**, *26*, 1167-1172.

19) Silverman, R.B. DNA-Interactive Drugs. *The Organic Chemistry of Drug Design and Drug Action*, 2nd Edition; Burlington, MA, 2004; pp 234-366.

20) Todd, R.C., Lippard, S.J. Structure of duplex DNA containing the cisplatin 1,2-$\{Pt(NH_3)_2\}^{2+}$-d(GpG) cross-linkat 1.77 Å resolution. *J. Inorg. Biochem*. **2010**, *104*, 902-908. Visualized with The PyMOL Molecular Graphics System, Version 1.3 Schrödinger, LLC.

21) Fu, D., Calvo, J.A., Samso, L.D. Balancing repair and tolerance of DNA damage caused by alkylating agents. *Nature Reviews Cancer*. **2012**, *12*, 104-120.

22) Collie, Gavin W.; Parkinson, Gary N. The application of DNA and RNA G-quadruplexes to therapeutic medicines. *Chem. Soc. Rev*. **2011**, *40*, 5867-5892.

23) Sen, D.; Gilbert, W. Formation of Parallel Four-Stranded Complexes by Guanine-Rich Motifs in DNA and its Implications for Meiosis *Nature.* **1988**, *334*, 364-366.

24) Neidle, S. The structures of quadruplex nucleic acids and their drug complexes. *Curr. Opinion Structural Biol*. **2009**, *19*, 239-250.

25) Sundquist, W. D.; Klug, A. Telomeric DNA Dimerizes by formation of Guanine Tetrads Between Hairpin Loops. *Nature.* **1989**, *342*, 82-829.

26) Huppert, J.L., Balasubramanian, S. Prevalence of quadruplexes in the human genome. *Nuc. Acids Res*. **2005**, *33*, 2908-2916.

27) Thi Le, T.V., Han, S., Chae., J., Park, H. G-Quadruplex Binding Ligands: from Naturally Occurring to Rationally Designed Molecules. *Curr. Pharm. Design*. **2012**, *18*, 1948-1972.

28) Han, F. X.; Wheelhouse, R. T.; Hurley, L. H. Interactions of TMPyP4 and TMPyP2 With Quadruplex DNA. Structural Basis For The Differential Effects On Telomerase Inhibition. *J. Am. Chem. Soc*. **1999**, *121*, 3561-3570.

29) Hurley, L. H.; Wheelhouse, R. T.; Sun, D.; Kerwin, S. M.; Salazar, M.; Fedoroff, O. Y.; Han, F. H.; Han, H.; Izbicka, E.; Von Hoff, D. D. G-quadruplexes As Targets For Drug Design. *Pharmacol. Therapeutics*, **2000**, *85*, 141-158.

30) Koeppel, F.; Riou, J-F.; Laoui, A.; Mailliet, P.; Arimondo, P. B.; Labit, D.; Petitgenet, O.; Hélène, C.; Mergny, J-L. Ethidium Derivatives Bind to G-quartets, Inhibit Telomerase And Act As Fluorescent Probes For Quadruplexes. *Nuc. Acids Res*., **2001**, *29*, 1087-1096.

31) Mergny, J-L.; Lacroix, L.; Teulade-Fichou, M-P.; Hounsou, C.; Guittat, L.; Hoarau, M.; Arimondo, P. B.; Vigneron, J-P.; Lehn, J-M.; Riou. J-F.; Garestier, T.; Hélène, C. Telomerase Inhibitors Based On Quadruplex Ligands Selected By A Fluorescence Assay. *Proc. Nat. Acad. Sci*. **2001**, *98*, 3062-3067.

32) Cocco,M. J.; L. A. Hanakahi; Huber, M. D.; Maizels, N. Specific Interactions Of Distamycin With G-quadruplex DNA. *Nuc. Acids Res.* **2003**, *31*, 2944-2951.

33) Ren, J.; Chaires, J. B. Sequence and Structural Selectivity of Nucleic Acid Binding Ligands. *Biochemistry*. **1999**, *38*, 16067-16075.

34) Agbandje, M.; Jenkins, T. C.; McKenna, R.; Reszka, A. P.; Neidle, S. D. Anthracene-9,10-diones as Potential Anticancer Agents. Synthesis, DNA-Binding, and Biological Studies on a Series of 2,6-Disubstituted Derivatives. *J. Med. Chem*. **1992**, *35*, 1418-1429.

35) Collier, D. A.; Neidle, S. D. Synthesis, Molecular Modeling, DNA Binding, and Antitumor Properties of Some Substituted Amidoanthraquinones. *J . Med. Chem.* **1988**, *31*, 847-857.

36) Tanious, F. A.; Jenkins T. C.; Neidle, S. D.; Wilson, W. D. Substituent Position Dictates the Intercalative DNA-Binding Mode for Anthracene-9,10-dione Antitumor Drugs. *Biochemistry.* **1992**, *31*, 11632-11640.

37) Han, F. X.; Wheelhouse, R. T.; Hurley, L. H. Interactions of TMPyP4 and TMPyP2 With Quadruplex DNA. Structural Basis For The Differential Effects On Telomerase Inhibition. *J. Am. Chem. Soc*. **1999**, *121*, 3561-3570.

38) a.)Mosher, M. D.; Natale, N. R. The Preparation of Intercalating Isoxazoles via a Nitrile Oxide Cycloadditon. *J. Heterocycl. Chem*. **1995**, *32*, 779-781. b.) Han, Xiaochun; Li, Chun; Mosher, Michael D.; Rider, Kevin C.; Zhou, Peiwen; Crawford, Ronald L.; Fusco, William; Paszczynski, Andrzej; Natale, Nicholas R. Design, synthesis and biological evaluation of a novel class of anticancer agents: Anthracenylisoxazole lexitropsin conjugates. *Bioorg. Med. Chem*. **2009**, *17*, 1671-1680.

39) Mirzaei, Y.R., Weaver, M.J., Steiger S.A., Kearns, A.K., Gajewski, M.P., Rider, K.C., Beall, H.D., Natale N.R. Improved synthesis of 3-aryl isoxazoles containing fused aromatic rings. *Tetrahedron*. **2012**, *68*, 10360-10364.

40) Han, X., Twamley, B., Natale N.R. Preparation of 3-(10'-Halo-9'-anthracenyl) Isoxazolecarboxylic Esters. *J. Heterocycl. Chem.* ***2003***, *40*, 539-545.

41) Cakmak, O., Aydogan, L., Berkil, K., Gulcin, I., Buyukgungor, O. Hight brominated anthracenes as precursors for the convenient synthesis of 2,9,10-trisubstituted anthracene derivaties. *Beilstein Journal of Organic Chemistry*. **2008**, *50*.

42) Gore, P.H., Gupta, S.D., Obaji, G.A. Anomalous Reactions of Cyanide with Two Hindered Aromatic Aldehydes. *J. praktische Chemie*. **1984**, *3*, 381-384.

43) Vellis, P.D., Mikroyannidis, D.A., Bagnis, D., Valentini, L., Kenny, J.M. New Anthracene-Containing Phenylene- or Thienylene-Vinylene Copolymers: Synthesis, Characterization, Photophysics, and Photovoltaics. *J. Applied Polymer Sci*. **2009**, *113*, 1173-1181.

44) Qu, X.; Trent, J.; Fokt, I.; Priebe, W.; Chaires, J. Allosteric, Chiral-selective Drug Binding to DNA. *Proc. Nat Acad. Sci.* **2000**, *97*, 12032-12037.

45) Waring, M. Facilitating Structural Transitions in DNA. *PNAS*, **2000**, *97*, 11685-11687.

46) Wilson, W. D.; Wang, Y-H.; Kusuma, S.; Chandraskaran, S.; Yang, N. C.; Boykin, D. W. The Effect of Intercalator Structure on Binding Strength and Base-Pair Specificity in DNA Interactions. *Biophys. Chem*. **1986**, *24*, 101-109.

Figure 16. NMR spectrum of 10-Bromoanthracene-9-carbaldehyde

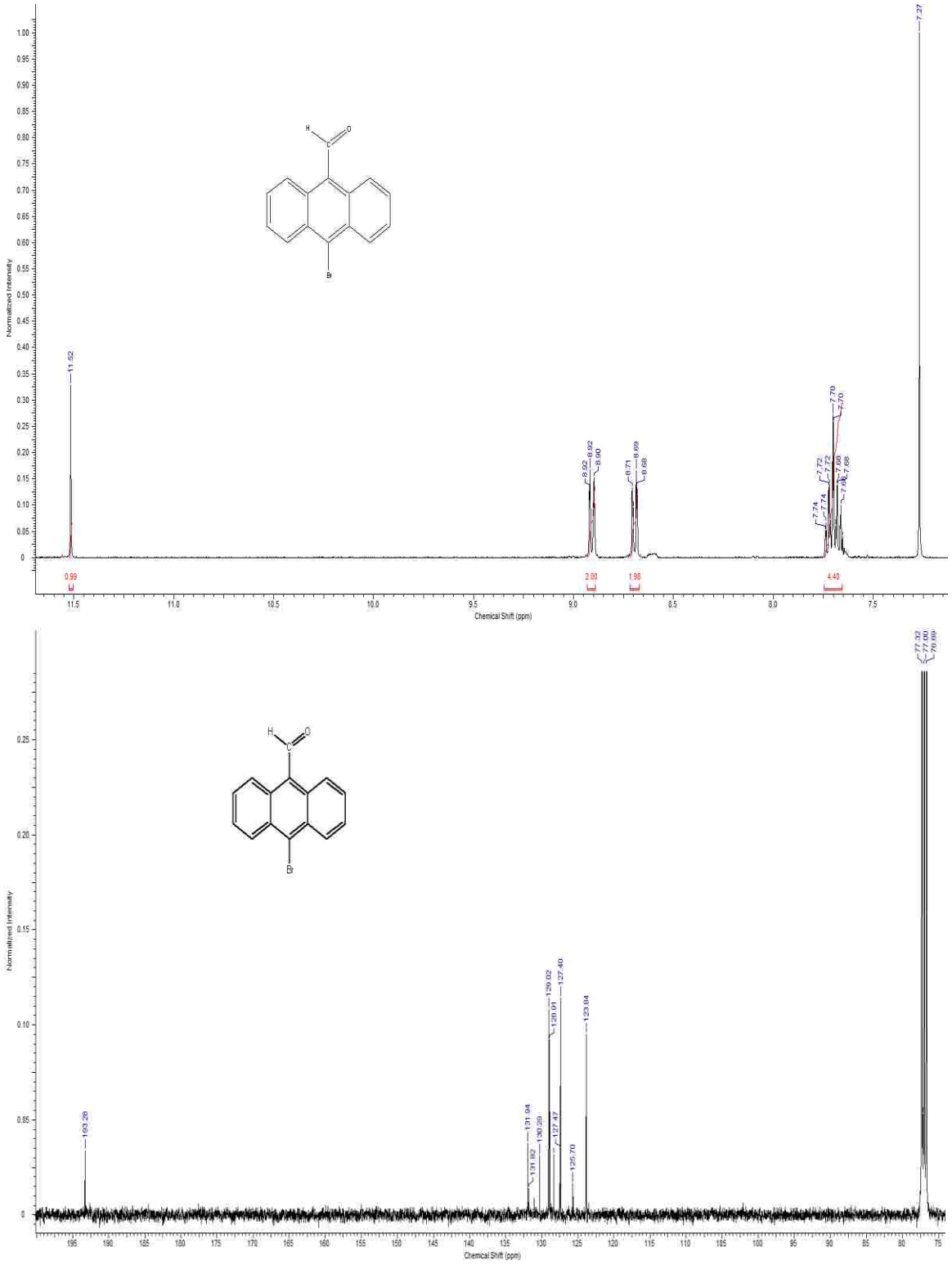

Figure 17. NMR spectrum of 10-Methoxyanthracene-9-carbaldehyde

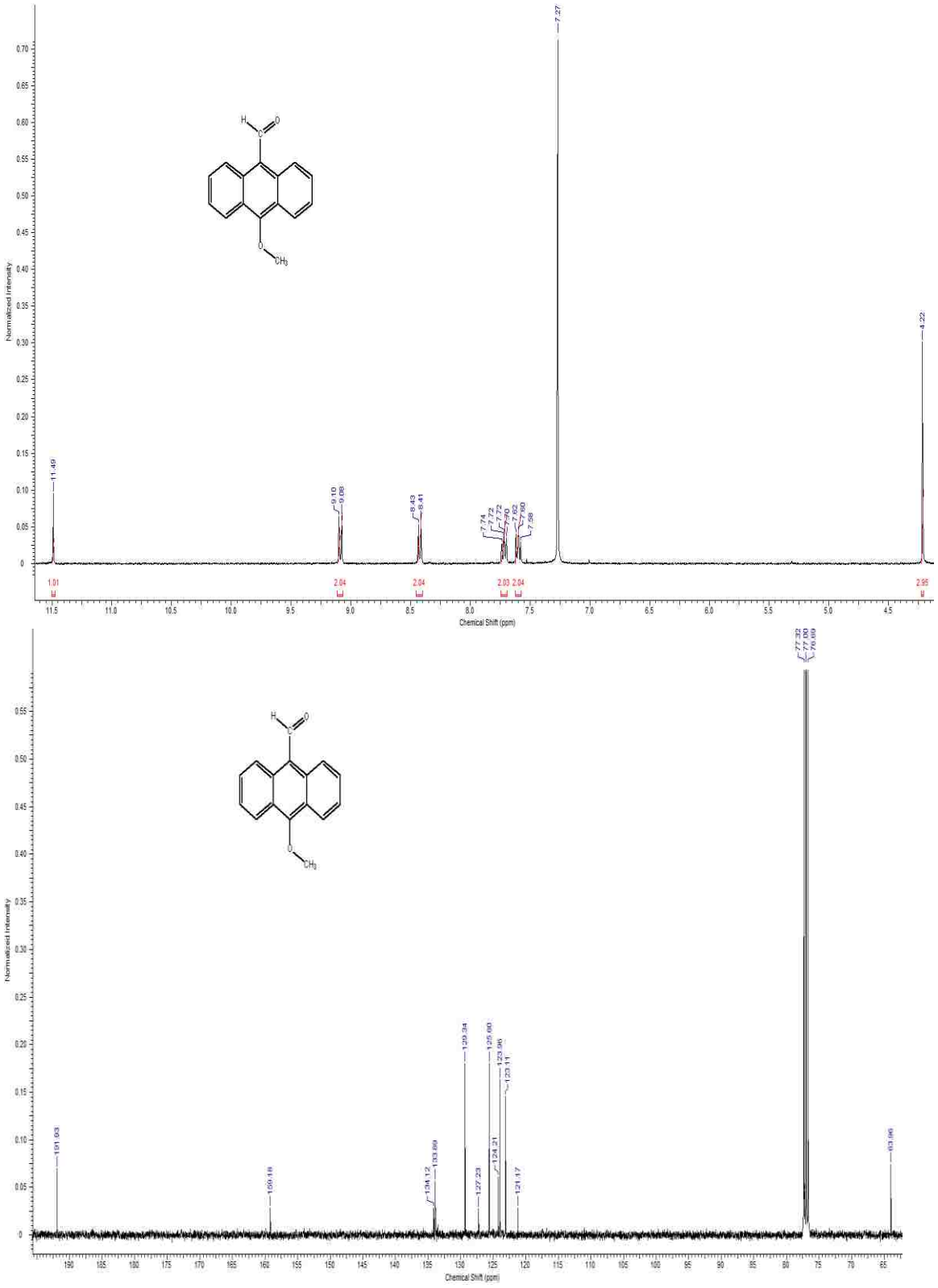

Figure 18. NMR spectrum of 10-Methoxyanthracene-9-carbaldehyde oxime

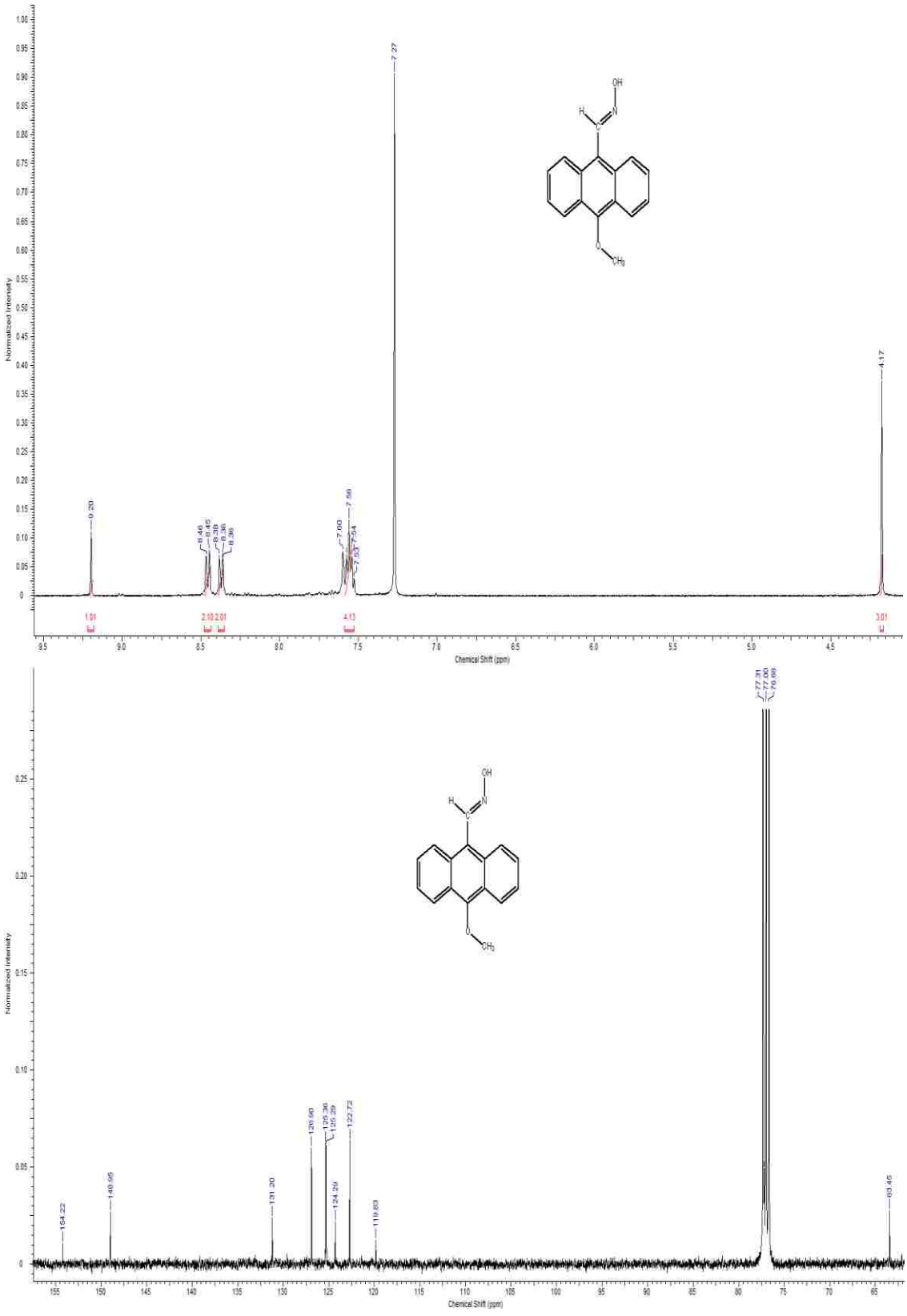

Figure 19. NMR spectrum of Ethyl 3-(10-methoxyanthracen-9-yl)-5-methylisoxazole-4-carboxylate

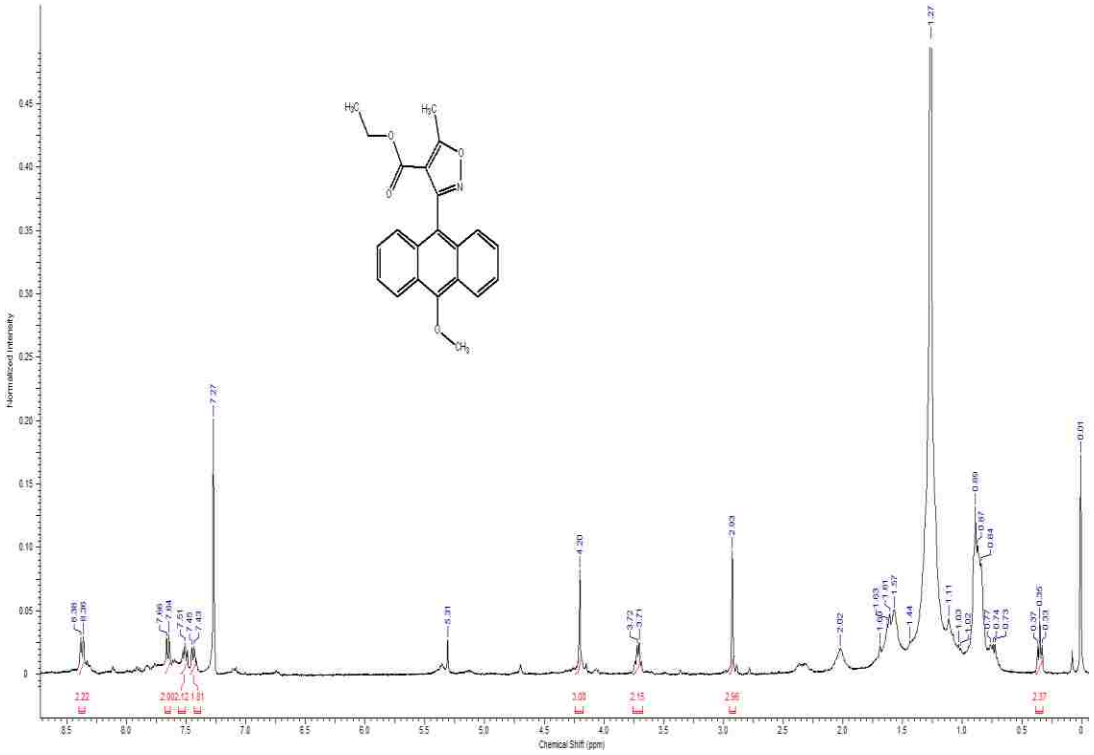

Figure 20. NMR spectrum of Anthracene-9-carbaldehyde oxime

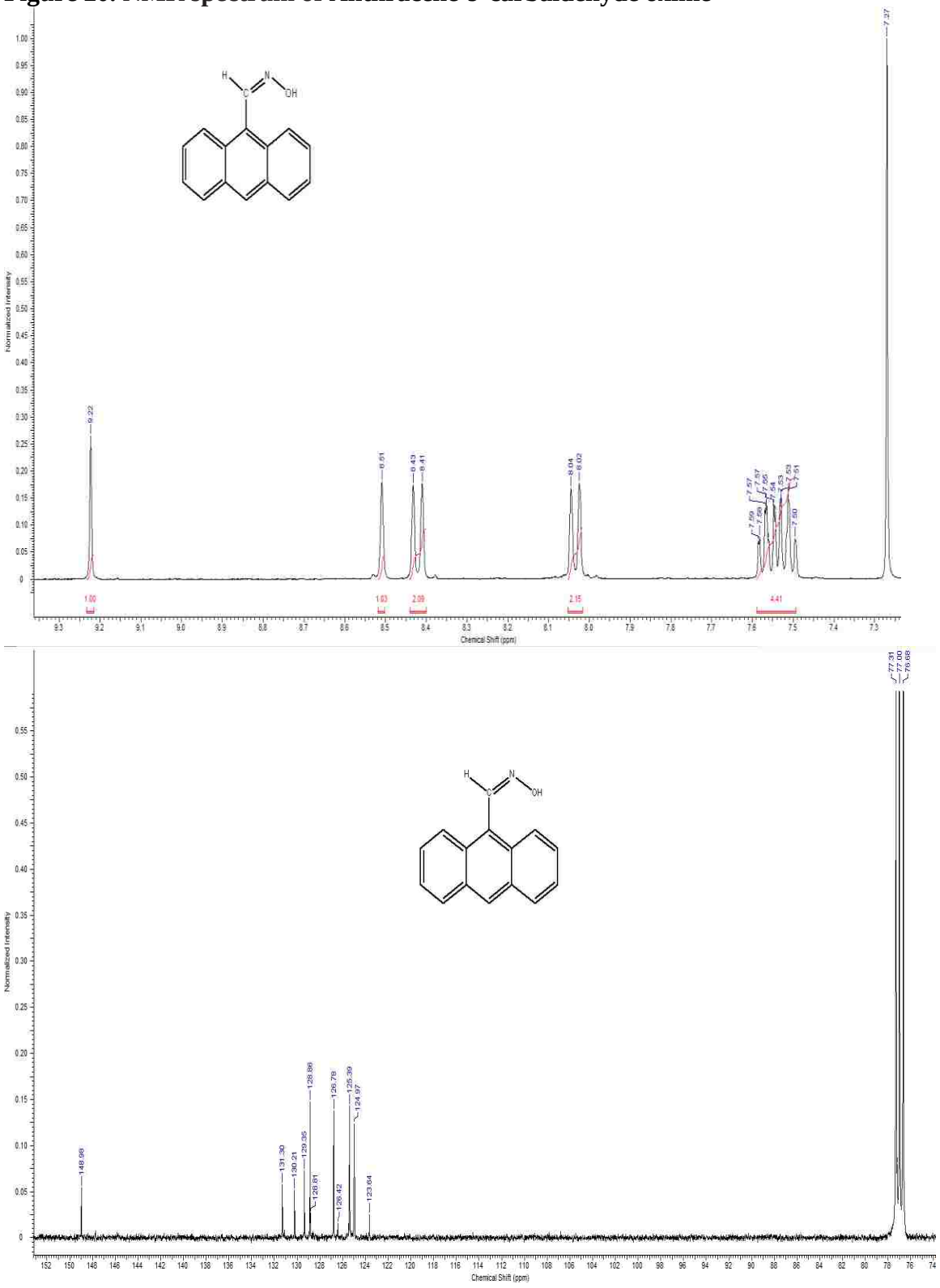

Figure 21. NMR spectrum of Ethyl 3-(anthracen-9-yl)-5-methylisoxazole-4-carboxylate

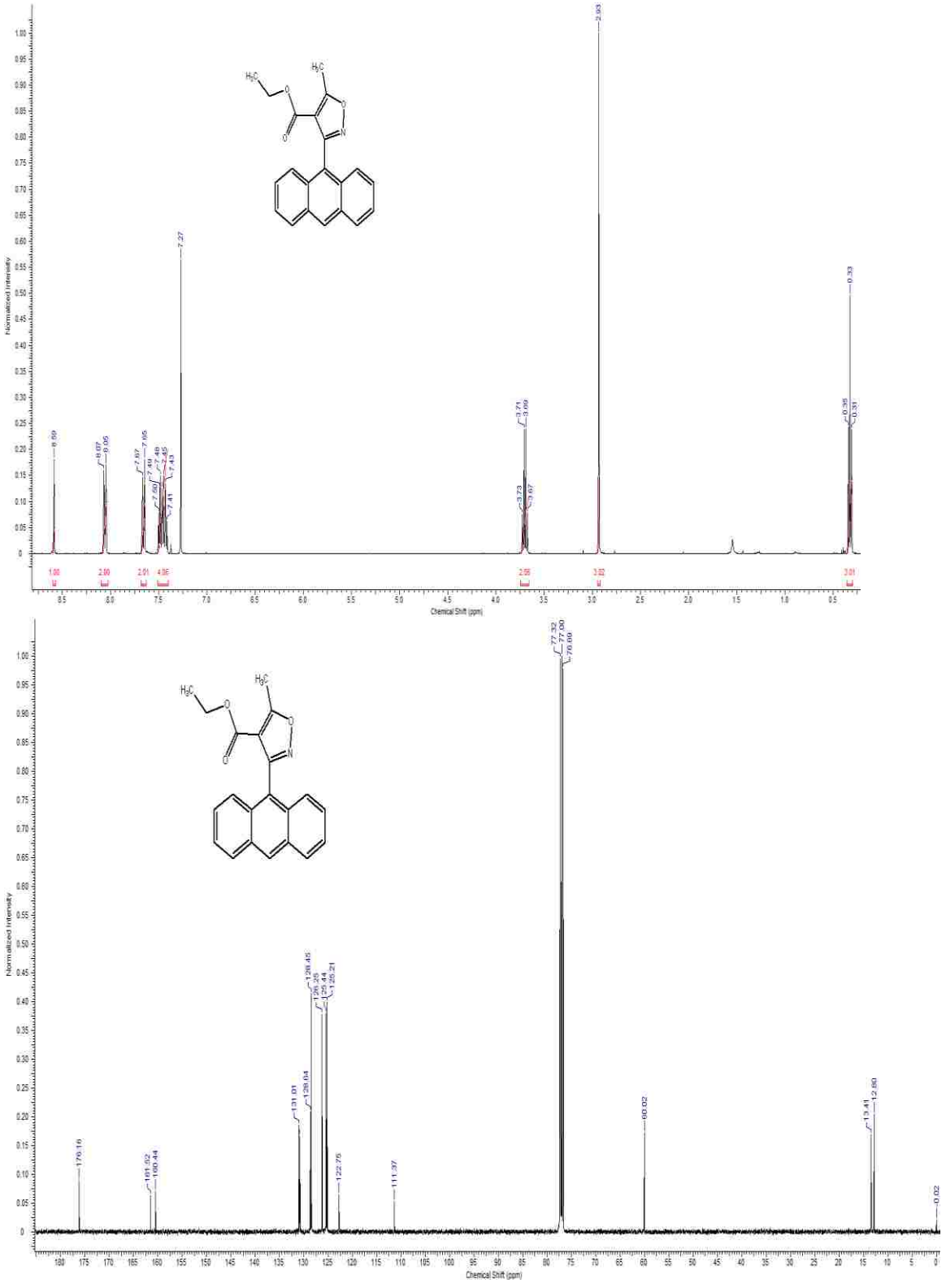

Figure 22. NMR spectrum of Ethyl 3-(10-chloroanthracen-9-yl)-5-methylisoxazole-4-carboxylate

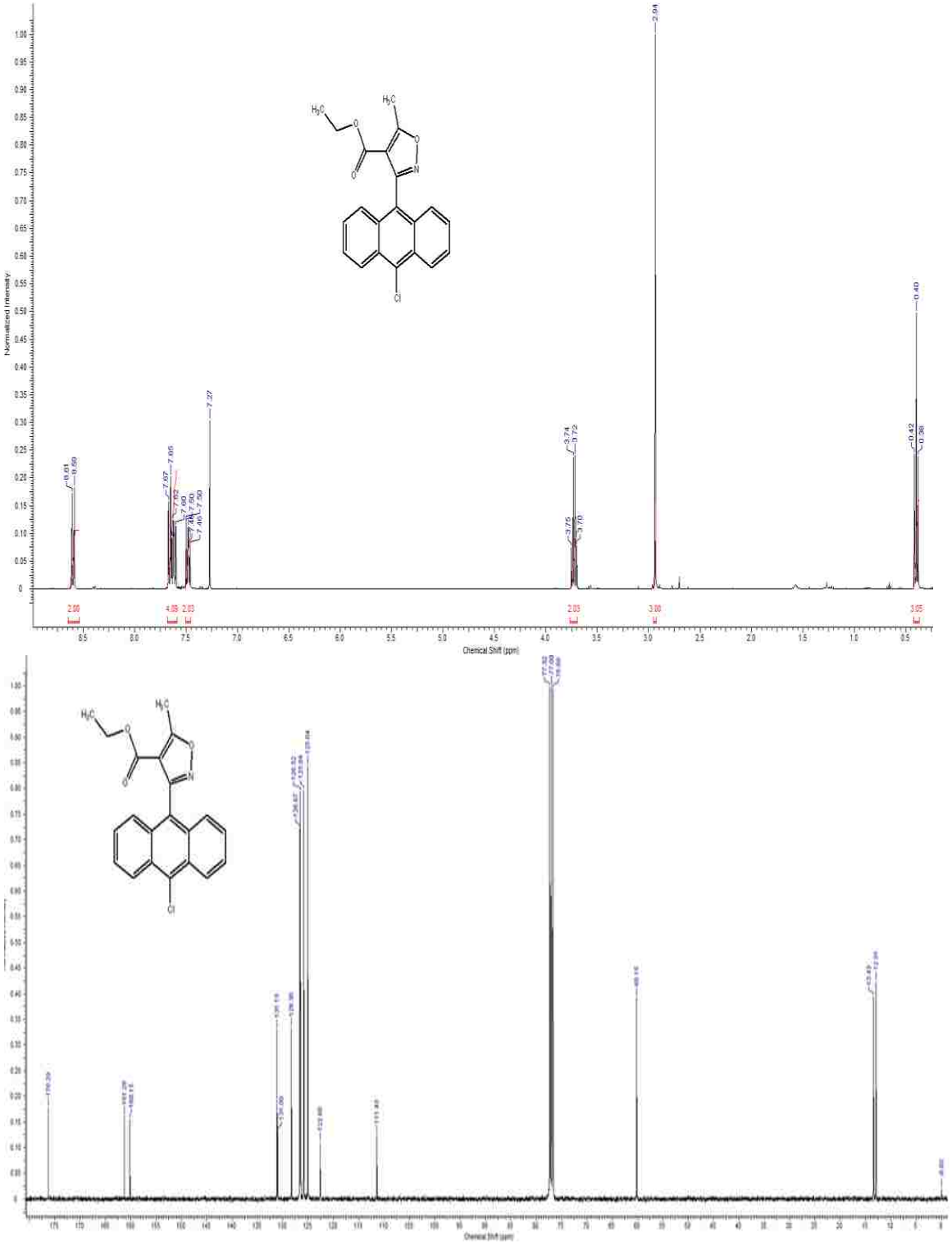

Figure 23. NMR spectrum of Ethyl 3-(9-chloro-10-oxo-9,10-dihydroanthracen-9-yl)-5-methylisoxazole-4-carboxylate

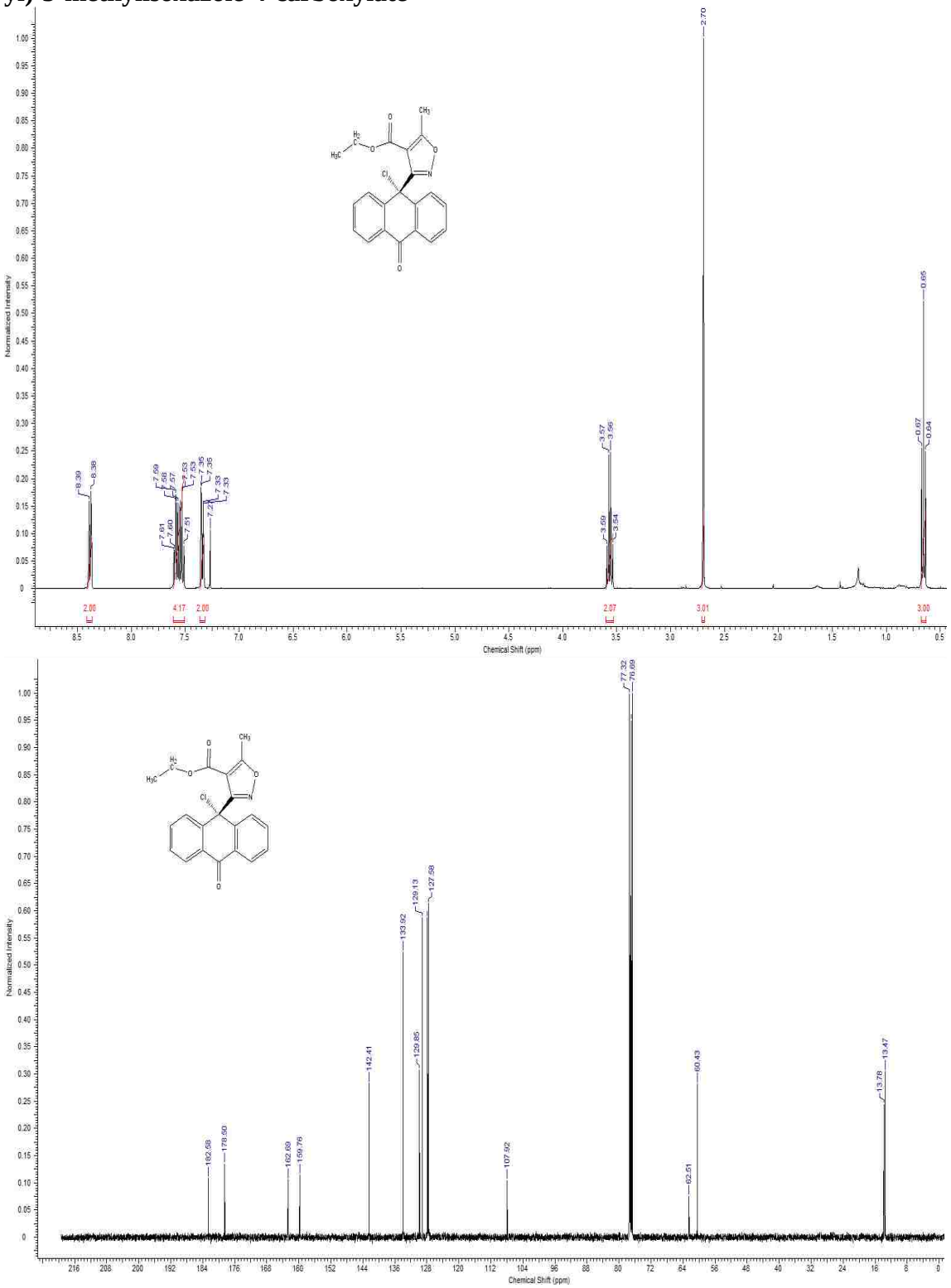

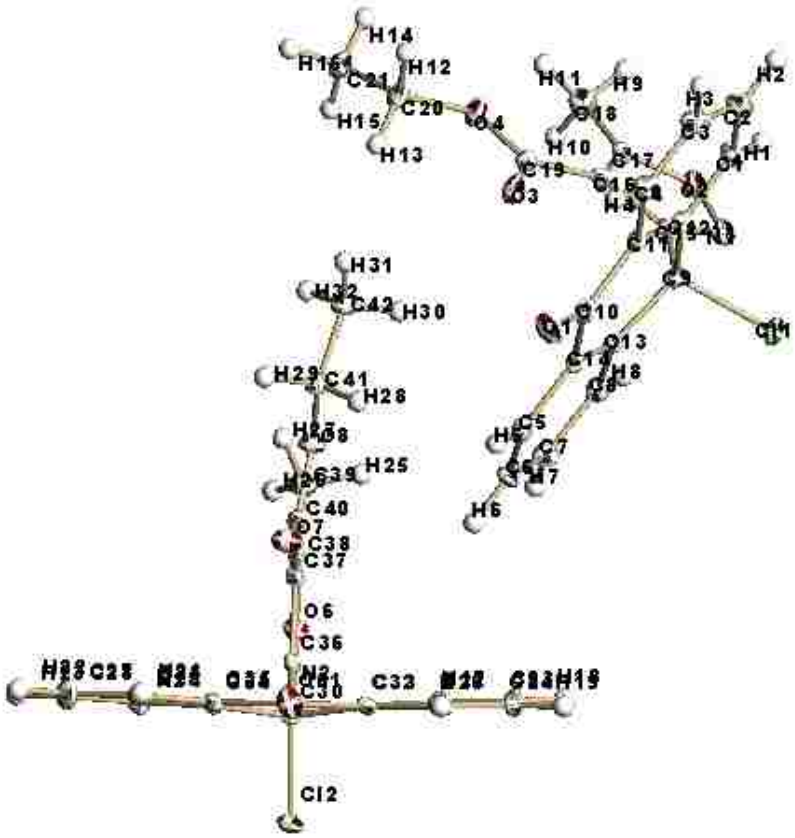

Figure 14.

Experimental details

Crystal data	
Chemical formula	$C_{43}H_{33}Cl_2NO_8$
M_r	762.60
Crystal system, space group	Triclinic, *P*1
Temperature (K)	100
a, *b*, *c* (Å)	10.014 (18), 12.57 (2), 14.97 (3)
α, β, γ (°)	78.09 (6), 73.36 (3), 89.01 (3)
V (Å^3)	1765 (6)
Z	2
Radiation type	?, λ = 0.71073 Å
μ (mm^{-1})	0.24
Crystal size (mm)	0.20 × 0.20 × 0.20
Data collection	

Diffractometer	?
Absorption correction	Multi-scan *SADABS* V2012/1 (Bruker AXS Inc.)
T_{min}, T_{max}	0.87, 0.95
No. of measured, independent and observed [$I > 2\sigma(I)$] reflections	21846, 8589, 6877
R_{int}	0.030
$(\sin \theta/\lambda)_{max}$ (Å^{-1})	0.682
Refinement	
$R[F^2 > 2\sigma(F^2)]$, $wR(F^2)$, S	0.039, 0.109, 1.11
No. of reflections	8589
No. of parameters	491
No. of restraints	0
H-atom treatment	H atoms treated by a mixture of independent and constrained refinement
$(\Delta/\sigma)_{max}$	0.530
$\Delta\rho_{max}$, $\Delta\rho_{min}$ (e Å^{-3})	0.45, −0.22

Computer programs: *SAINT* V8.27B (Bruker AXS Inc., 2012), *SHELXS97* (Sheldrick, 2008), *SHELXL97* (Sheldrick, 2008).

Computing details

Cell refinement: *SAINT* V8.27B (Bruker AXS Inc., 2012); data reduction: *SAINT* V8.27B (Bruker AXS Inc., 2012); program(s) used to solve structure: *SHELXS97* (Sheldrick, 2008); program(s) used to refine structure: *SHELXL97* (Sheldrick, 2008).

Experimental (I)

Crystal data

$C_{43}H_{33}Cl_2NO_8$	$Z = 2$
$M_r = 762.60$	$F(000) = 792$
Triclinic, $P\overline{1}$	$D_x = 1.436$ Mg m^{-3}
$a = 10.014$ (18) Å	? radiation, $\lambda = 0.71073$ Å
$b = 12.57$ (2) Å	Cell parameters from 9917 reflections
$c = 14.97$ (3) Å	$\theta = 2.2$–$28.8°$
$\alpha = 78.09$ (6)°	$\mu = 0.24$ mm^{-1}
$\beta = 73.36$ (3)°	$T = 100$ K

$\gamma = 89.01\ (3)°$	Prism
$V = 1765\ (6)\ Å^3$	0.20 × 0.20 × 0.20 mm

Data collection

Detector resolution: 8.3333 pixels mm^{-1}	$R_{int} = 0.030$
Absorption correction: multi-scan *SADABS* V2012/1 (Bruker AXS Inc.)	$\theta_{max} = 29.0°$, $\theta_{min} = 1.5°$
$T_{min} = 0.87$, $T_{max} = 0.95$	$h = -13 \rightarrow 13$
21846 measured reflections	$k = -17 \rightarrow 16$
8589 independent reflections	$l = -20 \rightarrow 20$
6877 reflections with $I > 2\sigma(I)$	

Refinement

Refinement on F^2	Primary atom site location: structure-invariant direct methods
Least-squares matrix: full	Secondary atom site location: difference Fourier map
$R[F^2 > 2\sigma(F^2)] = 0.039$	Hydrogen site location: inferred from neighbouring sites
$wR(F^2) = 0.109$	H atoms treated by a mixture of independent and constrained refinement
$S = 1.11$	$w = 1/[\sigma^2(F_o^2) + (0.060P)^2]$ where $P = (F_o^2 + 2F_c^2)/3$
8589 reflections	$(\Delta/\sigma)_{max} = 0.530$
491 parameters	$\Delta\rho_{max} = 0.45$ e $Å^{-3}$
0 restraints	$\Delta\rho_{min} = -0.22$ e $Å^{-3}$

Special details

Refinement

Refinement of F^2 against ALL reflections. The weighted *R*-factor *wR* and goodness of fit *S* are based on F^2, conventional *R*-factors *R* are based on *F*, with *F* set to zero for negative F^2. The threshold expression of $F^2 > \sigma(F^2)$ is used only for calculating *R*-factors(gt) *etc*. and is not relevant to the choice of reflections for refinement. *R*-factors based on F^2 are statistically about twice as large as those based on *F*, and *R*- factors based on ALL data will be even larger.

Fractional atomic coordinates and isotropic or equivalent isotropic displacement parameters (Å^2)

	x	*y*	*z*	U_{iso}*/U_{eq}
Cl1	0.39467 (4)	−0.13787 (3)	0.41774 (3)	0.01734 (10)
Cl2	0.89937 (4)	0.66479 (3)	0.42670 (3)	0.01629 (9)
C1	0.35916 (16)	−0.16673 (12)	0.21644 (11)	0.0170 (3)
H1	0.2771	−0.2021	0.2618	0.02*
C2	0.41980 (16)	−0.20648 (13)	0.13527 (11)	0.0194 (3)
H2	0.3805	−0.2701	0.1259	0.023*
C3	0.53801 (16)	−0.15387 (13)	0.06732 (11)	0.0190 (3)
H3	0.5781	−0.1805	0.011	0.023*
C4	0.59699 (16)	−0.06301 (13)	0.08184 (11)	0.0169 (3)
H4	0.6778	−0.0272	0.0353	0.02*
C5	0.59779 (16)	0.20976 (12)	0.27859 (11)	0.0156 (3)
H5	0.6837	0.241	0.2352	0.019*
C6	0.53337 (16)	0.25573 (12)	0.35502 (11)	0.0176 (3)
H6	0.5753	0.3179	0.3648	0.021*
C7	0.40673 (17)	0.21076 (13)	0.41786 (11)	0.0186 (3)
H7	0.3609	0.2435	0.4697	0.022*
C8	0.34743 (16)	0.11879 (12)	0.40524 (11)	0.0161 (3)
H8	0.261	0.0884	0.4485	0.019*
C9	0.35237 (15)	−0.03612 (11)	0.32323 (10)	0.0119 (3)
C10	0.60597 (15)	0.07311 (12)	0.17908 (10)	0.0136 (3)
C11	0.53872 (15)	−0.02303 (12)	0.16456 (10)	0.0124 (3)
C12	0.41784 (15)	−0.07508 (11)	0.23187 (10)	0.0121 (3)
C13	0.41347 (15)	0.07022 (11)	0.32949 (10)	0.0113 (3)
C14	0.53782 (15)	0.11751 (11)	0.26438 (10)	0.0119 (3)
C15	0.19528 (15)	−0.03352 (11)	0.34531 (10)	0.0119 (3)
C16	0.11564 (15)	0.03388 (12)	0.29156 (10)	0.0124 (3)
C17	−0.01974 (15)	0.00798 (12)	0.34468 (10)	0.0135 (3)
C18	−0.15775 (15)	0.04669 (13)	0.33728 (12)	0.0197 (3)
H9	−0.2266	−0.0146	0.3613	0.029*
H11	−0.1511	0.0779	0.2704	0.029*
H10	−0.1867	0.1024	0.3753	0.029*
C19	0.17127 (15)	0.11453 (12)	0.20198 (10)	0.0132 (3)
C20	0.11554 (16)	0.25119 (13)	0.08400 (11)	0.0188 (3)
H12	0.1443	0.2184	0.027	0.023*
H13	0.1957	0.2949	0.0857	0.023*

C21	−0.00676 (17)	0.32187 (13)	0.08050 (12)	0.0206 (3)
H14	−0.0875	0.2767	0.0838	0.031*
H16	0.0173	0.3767	0.0208	0.031*
H15	−0.0296	0.3582	0.1347	0.031*
C22	0.85760 (16)	0.41858 (12)	0.40063 (10)	0.0152 (3)
H17	0.7694	0.4256	0.444	0.018*
C23	0.92109 (16)	0.32023 (12)	0.40860 (11)	0.0174 (3)
H18	0.8765	0.2597	0.457	0.021*
C24	1.05042 (17)	0.31006 (12)	0.34561 (11)	0.0177 (3)
H19	1.0961	0.2433	0.3525	0.021*
C25	1.11295 (16)	0.39706 (12)	0.27278 (11)	0.0152 (3)
H20	1.2003	0.3891	0.2288	0.018*
C26	1.10150 (15)	0.77518 (12)	0.09529 (11)	0.0150 (3)
H21	1.1859	0.7652	0.0493	0.018*
C27	1.03694 (16)	0.87226 (13)	0.08403 (11)	0.0185 (3)
H22	1.0771	0.9295	0.0309	0.022*
C28	0.91269 (16)	0.88644 (12)	0.15061 (11)	0.0189 (3)
H23	0.868	0.9536	0.143	0.023*
C29	0.85343 (16)	0.80285 (12)	0.22823 (11)	0.0164 (3)
H24	0.7676	0.8127	0.2729	0.02*
C30	0.85690 (15)	0.61725 (11)	0.32927 (10)	0.0113 (3)
C31	1.11608 (15)	0.58694 (12)	0.18297 (10)	0.0131 (3)
C32	1.04862 (15)	0.49630 (12)	0.26351 (10)	0.0123 (3)
C33	0.92176 (15)	0.50795 (11)	0.32941 (10)	0.0116 (3)
C34	0.91894 (15)	0.70497 (12)	0.24094 (10)	0.0120 (3)
C35	1.04392 (15)	0.69082 (11)	0.17394 (10)	0.0119 (3)
C36	0.69982 (15)	0.60498 (11)	0.35216 (10)	0.0109 (3)
C37	0.62199 (15)	0.56608 (11)	0.29806 (10)	0.0129 (3)
C38	0.48620 (15)	0.56731 (11)	0.35019 (10)	0.0131 (3)
C39	0.34938 (15)	0.53651 (13)	0.34072 (11)	0.0184 (3)
H25	0.321	0.462	0.3767	0.028*
H27	0.3573	0.5406	0.2733	0.028*
H26	0.2794	0.5866	0.3659	0.028*
C40	0.68012 (15)	0.53118 (12)	0.20702 (10)	0.0127 (3)
C41	0.63080 (16)	0.44355 (13)	0.09360 (10)	0.0161 (3)
H28	0.708	0.3939	0.0965	0.019*
H29	0.6647	0.5049	0.0383	0.019*
C42	0.50717 (16)	0.38379 (13)	0.08488 (11)	0.0185 (3)

H30	0.4796	0.32	0.1374	0.028*
H31	0.5326	0.3602	0.0239	0.028*
H32	0.4291	0.4323	0.0876	0.028*
N1	0.11438 (12)	−0.09462 (10)	0.42317 (9)	0.0147 (3)
N2	0.61807 (12)	0.62767 (10)	0.43052 (9)	0.0141 (3)
O1	0.71551 (11)	0.11532 (9)	0.12176 (8)	0.0213 (3)
O2	−0.02303 (10)	−0.06859 (8)	0.42289 (7)	0.0161 (2)
O3	0.29466 (11)	0.13287 (9)	0.16269 (7)	0.0192 (2)
O4	0.07022 (11)	0.16608 (9)	0.17063 (7)	0.0180 (2)
O5	1.22729 (11)	0.57605 (9)	0.12509 (8)	0.0203 (2)
O6	0.48084 (10)	0.60448 (8)	0.42934 (7)	0.0149 (2)
O7	0.80195 (11)	0.54218 (9)	0.16192 (7)	0.0191 (2)
O8	0.58166 (10)	0.48367 (9)	0.18180 (7)	0.0159 (2)

Atomic displacement parameters (Å^2)

	U^{11}	U^{22}	U^{33}	U^{12}	U^{13}	U^{23}
Cl1	0.01769 (19)	0.01571 (18)	0.01612 (19)	0.00367 (14)	−0.00459 (15)	0.00155 (14)
Cl2	0.01699 (19)	0.01912 (19)	0.01480 (18)	−0.00256 (14)	−0.00484 (14)	−0.00744 (14)
C1	0.0149 (8)	0.0155 (7)	0.0189 (8)	−0.0018 (6)	−0.0008 (6)	−0.0052 (6)
C2	0.0187 (8)	0.0180 (8)	0.0246 (8)	0.0008 (6)	−0.0065 (7)	−0.0109 (7)
C3	0.0176 (8)	0.0238 (8)	0.0177 (8)	0.0046 (6)	−0.0035 (6)	−0.0117 (7)
C4	0.0139 (7)	0.0195 (8)	0.0158 (8)	0.0015 (6)	−0.0017 (6)	−0.0042 (6)
C5	0.0151 (7)	0.0121 (7)	0.0196 (8)	−0.0004 (6)	−0.0066 (6)	−0.0010 (6)
C6	0.0223 (8)	0.0120 (7)	0.0230 (8)	0.0006 (6)	−0.0116 (7)	−0.0065 (6)
C7	0.0215 (8)	0.0196 (8)	0.0177 (8)	0.0053 (6)	−0.0073 (7)	−0.0089 (6)
C8	0.0151 (8)	0.0183 (8)	0.0143 (7)	0.0018 (6)	−0.0031 (6)	−0.0042 (6)
C9	0.0116 (7)	0.0113 (7)	0.0114 (7)	0.0018 (5)	−0.0026 (6)	0.0000 (5)
C10	0.0123 (7)	0.0125 (7)	0.0145 (7)	0.0019 (6)	−0.0033 (6)	−0.0006 (6)
C11	0.0111 (7)	0.0125 (7)	0.0133 (7)	0.0025 (5)	−0.0032 (6)	−0.0026 (6)
C12	0.0122 (7)	0.0111 (7)	0.0125 (7)	0.0034 (5)	−0.0028 (6)	−0.0029 (6)
C13	0.0117 (7)	0.0106 (7)	0.0126 (7)	0.0022 (5)	−0.0051 (6)	−0.0024 (5)
C14	0.0115 (7)	0.0098 (7)	0.0143 (7)	0.0029 (5)	−0.0048 (6)	−0.0011 (6)
C15	0.0137 (7)	0.0094 (7)	0.0118 (7)	0.0010 (5)	−0.0014 (6)	−0.0039 (5)
C16	0.0118 (7)	0.0123 (7)	0.0134 (7)	0.0007 (6)	−0.0030 (6)	−0.0041 (6)
C17	0.0156 (7)	0.0102 (7)	0.0145 (7)	−0.0009 (6)	−0.0035 (6)	−0.0032 (6)
C18	0.0116 (7)	0.0235 (8)	0.0230 (8)	0.0019 (6)	−0.0029 (6)	−0.0058 (7)
C19	0.0132 (7)	0.0142 (7)	0.0133 (7)	0.0025 (6)	−0.0044 (6)	−0.0051 (6)
C20	0.0188 (8)	0.0200 (8)	0.0142 (7)	0.0008 (6)	−0.0039 (6)	0.0029 (6)

C21	0.0203 (8)	0.0210 (8)	0.0210 (8)	0.0042 (7)	−0.0087 (7)	−0.0019 (7)
C22	0.0156 (7)	0.0153 (7)	0.0133 (7)	−0.0022 (6)	−0.0028 (6)	−0.0016 (6)
C23	0.0227 (8)	0.0126 (7)	0.0162 (7)	−0.0032 (6)	−0.0075 (6)	0.0014 (6)
C24	0.0229 (8)	0.0111 (7)	0.0229 (8)	0.0039 (6)	−0.0121 (7)	−0.0046 (6)
C25	0.0133 (7)	0.0156 (7)	0.0183 (8)	0.0006 (6)	−0.0051 (6)	−0.0066 (6)
C26	0.0118 (7)	0.0176 (7)	0.0148 (7)	−0.0026 (6)	−0.0029 (6)	−0.0023 (6)
C27	0.0184 (8)	0.0165 (8)	0.0169 (8)	−0.0033 (6)	−0.0038 (6)	0.0030 (6)
C28	0.0193 (8)	0.0131 (7)	0.0234 (8)	0.0017 (6)	−0.0066 (7)	−0.0011 (6)
C29	0.0140 (7)	0.0144 (7)	0.0188 (8)	0.0008 (6)	−0.0014 (6)	−0.0035 (6)
C30	0.0119 (7)	0.0125 (7)	0.0104 (7)	−0.0005 (5)	−0.0028 (6)	−0.0047 (6)
C31	0.0119 (7)	0.0142 (7)	0.0148 (7)	−0.0013 (6)	−0.0047 (6)	−0.0050 (6)
C32	0.0120 (7)	0.0119 (7)	0.0147 (7)	−0.0016 (5)	−0.0057 (6)	−0.0040 (6)
C33	0.0126 (7)	0.0112 (7)	0.0125 (7)	−0.0013 (5)	−0.0058 (6)	−0.0029 (6)
C34	0.0117 (7)	0.0113 (7)	0.0134 (7)	−0.0027 (5)	−0.0042 (6)	−0.0026 (6)
C35	0.0117 (7)	0.0113 (7)	0.0129 (7)	−0.0023 (5)	−0.0039 (6)	−0.0025 (6)
C36	0.0123 (7)	0.0076 (6)	0.0117 (7)	−0.0002 (5)	−0.0021 (6)	−0.0012 (5)
C37	0.0140 (7)	0.0108 (7)	0.0130 (7)	−0.0009 (6)	−0.0032 (6)	−0.0016 (6)
C38	0.0155 (7)	0.0103 (7)	0.0130 (7)	0.0000 (6)	−0.0040 (6)	−0.0012 (6)
C39	0.0121 (7)	0.0230 (8)	0.0196 (8)	−0.0010 (6)	−0.0039 (6)	−0.0043 (7)
C40	0.0135 (7)	0.0132 (7)	0.0111 (7)	0.0000 (6)	−0.0042 (6)	−0.0012 (6)
C41	0.0155 (8)	0.0219 (8)	0.0126 (7)	0.0019 (6)	−0.0041 (6)	−0.0073 (6)
C42	0.0187 (8)	0.0209 (8)	0.0186 (8)	0.0002 (6)	−0.0074 (6)	−0.0074 (6)
N1	0.0097 (6)	0.0147 (6)	0.0171 (6)	0.0007 (5)	−0.0008 (5)	−0.0021 (5)
N2	0.0099 (6)	0.0147 (6)	0.0164 (6)	−0.0025 (5)	−0.0012 (5)	−0.0040 (5)
O1	0.0176 (6)	0.0192 (6)	0.0212 (6)	−0.0062 (5)	0.0043 (5)	−0.0048 (5)
O2	0.0099 (5)	0.0159 (5)	0.0190 (6)	−0.0005 (4)	−0.0004 (4)	−0.0012 (4)
O3	0.0133 (5)	0.0226 (6)	0.0171 (6)	0.0014 (4)	−0.0021 (4)	0.0030 (5)
O4	0.0131 (5)	0.0197 (6)	0.0170 (6)	0.0005 (4)	−0.0036 (4)	0.0045 (4)
O5	0.0156 (6)	0.0189 (6)	0.0210 (6)	0.0003 (4)	0.0031 (5)	−0.0039 (5)
O6	0.0107 (5)	0.0171 (5)	0.0167 (5)	0.0003 (4)	−0.0017 (4)	−0.0061 (4)
O7	0.0139 (5)	0.0273 (6)	0.0168 (6)	−0.0021 (5)	−0.0019 (4)	−0.0097 (5)
O8	0.0132 (5)	0.0222 (6)	0.0144 (5)	−0.0010 (4)	−0.0038 (4)	−0.0084 (4)

Geometric parameters (Å, º)

Cl1—C9	1.842 (3)	C22—C23	1.379 (3)
Cl2—C30	1.840 (3)	C22—C33	1.396 (3)
C1—C2	1.383 (3)	C22—H17	0.95
C1—C12	1.391 (3)	C23—C24	1.388 (3)

C1—H1	0.95	C23—H18	0.95
C2—C3	1.390 (3)	C24—C25	1.385 (3)
C2—H2	0.95	C24—H19	0.95
C3—C4	1.378 (3)	C25—C32	1.394 (3)
C3—H3	0.95	C25—H20	0.95
C4—C11	1.399 (3)	C26—C27	1.373 (3)
C4—H4	0.95	C26—C35	1.400 (3)
C5—C6	1.377 (3)	C26—H21	0.95
C5—C14	1.396 (3)	C27—C28	1.389 (3)
C5—H5	0.95	C27—H22	0.95
C6—C7	1.391 (3)	C28—C29	1.389 (3)
C6—H6	0.95	C28—H23	0.95
C7—C8	1.379 (3)	C29—C34	1.388 (3)
C7—H7	0.95	C29—H24	0.95
C8—C13	1.392 (3)	C30—C33	1.509 (3)
C8—H8	0.95	C30—C36	1.514 (3)
C9—C13	1.511 (3)	C30—C34	1.517 (3)
C9—C15	1.513 (3)	C31—O5	1.225 (2)
C9—C12	1.514 (3)	C31—C35	1.482 (3)
C10—O1	1.230 (2)	C31—C32	1.483 (3)
C10—C11	1.477 (3)	C32—C33	1.394 (3)
C10—C14	1.479 (3)	C34—C35	1.397 (3)
C11—C12	1.402 (3)	C36—N2	1.307 (3)
C13—C14	1.395 (3)	C36—C37	1.428 (3)
C15—N1	1.310 (3)	C37—C38	1.362 (3)
C15—C16	1.436 (3)	C37—C40	1.474 (3)
C16—C17	1.366 (3)	C38—O6	1.347 (3)
C16—C19	1.472 (3)	C38—C39	1.483 (3)
C17—O2	1.346 (3)	C39—H25	0.98
C17—C18	1.484 (3)	C39—H27	0.98
C18—H9	0.98	C39—H26	0.98
C18—H11	0.98	C40—O7	1.208 (3)
C18—H10	0.98	C40—O8	1.341 (2)
C19—O3	1.210 (3)	C41—O8	1.460 (3)
C19—O4	1.337 (2)	C41—C42	1.510 (3)
C20—O4	1.462 (3)	C41—H28	0.99
C20—C21	1.507 (3)	C41—H29	0.99
C20—H12	0.99	C42—H30	0.98

C20—H13	0.99	C42—H31	0.98
C21—H14	0.98	C42—H32	0.98
C21—H16	0.98	N1—O2	1.410 (3)
C21—H15	0.98	N2—O6	1.415 (3)
C2—C1—C12	120.24 (16)	C22—C23—C24	119.75 (16)
C2—C1—H1	119.9	C22—C23—H18	120.1
C12—C1—H1	119.9	C24—C23—H18	120.1
C1—C2—C3	120.34 (17)	C25—C24—C23	120.12 (16)
C1—C2—H2	119.8	C25—C24—H19	119.9
C3—C2—H2	119.8	C23—C24—H19	119.9
C4—C3—C2	119.90 (17)	C24—C25—C32	120.44 (17)
C4—C3—H3	120.1	C24—C25—H20	119.8
C2—C3—H3	120.1	C32—C25—H20	119.8
C3—C4—C11	120.51 (16)	C27—C26—C35	120.53 (17)
C3—C4—H4	119.7	C27—C26—H21	119.7
C11—C4—H4	119.7	C35—C26—H21	119.7
C6—C5—C14	120.48 (17)	C26—C27—C28	119.75 (16)
C6—C5—H5	119.8	C26—C27—H22	120.1
C14—C5—H5	119.8	C28—C27—H22	120.1
C5—C6—C7	119.76 (16)	C27—C28—C29	120.30 (17)
C5—C6—H6	120.1	C27—C28—H23	119.9
C7—C6—H6	120.1	C29—C28—H23	119.9
C8—C7—C6	120.24 (16)	C34—C29—C28	120.37 (17)
C8—C7—H7	119.9	C34—C29—H24	119.8
C6—C7—H7	119.9	C28—C29—H24	119.8
C7—C8—C13	120.39 (17)	C33—C30—C36	110.70 (14)
C7—C8—H8	119.8	C33—C30—C34	115.52 (15)
C13—C8—H8	119.8	C36—C30—C34	111.86 (12)
C13—C9—C15	110.92 (13)	C33—C30—Cl2	104.31 (12)
C13—C9—C12	115.38 (14)	C36—C30—Cl2	108.80 (11)
C15—C9—C12	111.79 (13)	C34—C30—Cl2	105.01 (16)
C13—C9—Cl1	104.50 (15)	O5—C31—C35	120.93 (15)
C15—C9—Cl1	108.42 (11)	O5—C31—C32	121.13 (16)
C12—C9—Cl1	105.19 (16)	C35—C31—C32	117.94 (16)
O1—C10—C11	120.96 (16)	C25—C32—C33	119.39 (15)
O1—C10—C14	120.87 (16)	C25—C32—C31	119.16 (17)
C11—C10—C14	118.17 (15)	C33—C32—C31	121.44 (15)
C4—C11—C12	119.32 (16)	C32—C33—C22	119.57 (16)

C4—C11—C10	119.27 (15)	C32—C33—C30	121.18 (14)
C12—C11—C10	121.40 (16)	C22—C33—C30	119.13 (17)
C1—C12—C11	119.66 (16)	C29—C34—C35	119.27 (15)
C1—C12—C9	119.01 (15)	C29—C34—C30	119.49 (16)
C11—C12—C9	121.29 (15)	C35—C34—C30	121.19 (15)
C8—C13—C14	119.44 (16)	C34—C35—C26	119.78 (16)
C8—C13—C9	118.83 (15)	C34—C35—C31	121.35 (15)
C14—C13—C9	121.65 (15)	C26—C35—C31	118.86 (16)
C13—C14—C5	119.61 (16)	N2—C36—C37	111.56 (18)
C13—C14—C10	121.15 (15)	N2—C36—C30	120.83 (14)
C5—C14—C10	119.23 (15)	C37—C36—C30	127.58 (15)
N1—C15—C16	111.56 (18)	C38—C37—C36	104.65 (18)
N1—C15—C9	120.59 (14)	C38—C37—C40	129.08 (14)
C16—C15—C9	127.80 (14)	C36—C37—C40	126.26 (17)
C17—C16—C15	103.98 (17)	O6—C38—C37	109.06 (15)
C17—C16—C19	129.32 (14)	O6—C38—C39	115.39 (13)
C15—C16—C19	126.66 (16)	C37—C38—C39	135.54 (17)
O2—C17—C16	109.47 (15)	C38—C39—H25	109.5
O2—C17—C18	115.27 (13)	C38—C39—H27	109.5
C16—C17—C18	135.22 (17)	H25—C39—H27	109.5
C17—C18—H9	109.5	C38—C39—H26	109.5
C17—C18—H11	109.5	H25—C39—H26	109.5
H9—C18—H11	109.5	H27—C39—H26	109.5
C17—C18—H10	109.5	O7—C40—O8	124.38 (17)
H9—C18—H10	109.5	O7—C40—C37	123.99 (14)
H11—C18—H10	109.5	O8—C40—C37	111.61 (16)
O3—C19—O4	124.32 (17)	O8—C41—C42	106.17 (14)
O3—C19—C16	123.36 (14)	O8—C41—H28	110.5
O4—C19—C16	112.31 (16)	C42—C41—H28	110.5
O4—C20—C21	107.02 (15)	O8—C41—H29	110.5
O4—C20—H12	110.3	C42—C41—H29	110.5
C21—C20—H12	110.3	H28—C41—H29	108.7
O4—C20—H13	110.3	C41—C42—H30	109.5
C21—C20—H13	110.3	C41—C42—H31	109.5
H12—C20—H13	108.6	H30—C42—H31	109.5
C20—C21—H14	109.5	C41—C42—H32	109.5
C20—C21—H16	109.5	H30—C42—H32	109.5
H14—C21—H16	109.5	H31—C42—H32	109.5

C20—C21—H15	109.5	C15—N1—O2	105.50 (15)
H14—C21—H15	109.5	C36—N2—O6	105.34 (15)
H16—C21—H15	109.5	C17—O2—N1	109.49 (11)
C23—C22—C33	120.64 (18)	C19—O4—C20	116.30 (15)
C23—C22—H17	119.7	C38—O6—N2	109.39 (11)
C33—C22—H17	119.7	C40—O8—C41	115.37 (14)
C12—C1—C2—C3	−1.5 (2)	O5—C31—C32—C25	−0.4 (2)
C1—C2—C3—C4	1.4 (2)	C35—C31—C32—C25	178.88 (13)
C2—C3—C4—C11	−0.1 (2)	O5—C31—C32—C33	−179.71 (14)
C14—C5—C6—C7	−0.8 (2)	C35—C31—C32—C33	−0.4 (2)
C5—C6—C7—C8	1.7 (2)	C25—C32—C33—C22	−3.3 (2)
C6—C7—C8—C13	−0.1 (2)	C31—C32—C33—C22	176.02 (13)
C3—C4—C11—C12	−1.3 (2)	C25—C32—C33—C30	172.62 (13)
C3—C4—C11—C10	178.72 (14)	C31—C32—C33—C30	−8.1 (2)
O1—C10—C11—C4	−3.3 (2)	C23—C22—C33—C32	2.5 (2)
C14—C10—C11—C4	176.57 (13)	C23—C22—C33—C30	−173.48 (13)
O1—C10—C11—C12	176.69 (14)	C36—C30—C33—C32	142.29 (15)
C14—C10—C11—C12	−3.4 (2)	C34—C30—C33—C32	13.87 (19)
C2—C1—C12—C11	0.1 (2)	Cl2—C30—C33—C32	−100.84 (19)
C2—C1—C12—C9	−177.61 (14)	C36—C30—C33—C22	−41.77 (19)
C4—C11—C12—C1	1.2 (2)	C34—C30—C33—C22	−170.19 (13)
C10—C11—C12—C1	−178.76 (13)	Cl2—C30—C33—C22	75.1 (2)
C4—C11—C12—C9	178.92 (13)	C28—C29—C34—C35	−1.1 (2)
C10—C11—C12—C9	−1.1 (2)	C28—C29—C34—C30	176.39 (14)
C13—C9—C12—C1	−173.93 (13)	C33—C30—C34—C29	170.70 (13)
C15—C9—C12—C1	−45.95 (19)	C36—C30—C34—C29	42.85 (19)
Cl1—C9—C12—C1	71.50 (19)	Cl2—C30—C34—C29	−74.99 (18)
C13—C9—C12—C11	8.36 (19)	C33—C30—C34—C35	−11.90 (19)
C15—C9—C12—C11	136.33 (15)	C36—C30—C34—C35	−139.74 (15)
Cl1—C9—C12—C11	−106.21 (18)	Cl2—C30—C34—C35	102.41 (17)
C7—C8—C13—C14	−2.3 (2)	C29—C34—C35—C26	0.2 (2)
C7—C8—C13—C9	174.37 (13)	C30—C34—C35—C26	−177.26 (13)
C15—C9—C13—C8	43.18 (18)	C29—C34—C35—C31	−178.46 (13)
C12—C9—C13—C8	171.59 (13)	C30—C34—C35—C31	4.1 (2)
Cl1—C9—C13—C8	−73.44 (19)	C27—C26—C35—C34	0.8 (2)
C15—C9—C13—C14	−140.27 (15)	C27—C26—C35—C31	179.40 (14)
C12—C9—C13—C14	−11.87 (19)	O5—C31—C35—C34	−178.32 (14)
Cl1—C9—C13—C14	103.10 (19)	C32—C31—C35—C34	2.4 (2)

C8—C13—C14—C5	3.1 (2)	O5—C31—C35—C26	3.1 (2)
C9—C13—C14—C5	−173.44 (13)	C32—C31—C35—C26	−176.20 (13)
C8—C13—C14—C10	−175.52 (13)	C33—C30—C36—N2	114.47 (16)
C9—C13—C14—C10	8.0 (2)	C34—C30—C36—N2	−115.2 (2)
C6—C5—C14—C13	−1.6 (2)	Cl2—C30—C36—N2	0.40 (17)
C6—C5—C14—C10	177.06 (13)	C33—C30—C36—C37	−63.2 (2)
O1—C10—C14—C13	179.83 (13)	C34—C30—C36—C37	67.1 (2)
C11—C10—C14—C13	0.0 (2)	Cl2—C30—C36—C37	−177.30 (12)
O1—C10—C14—C5	1.2 (2)	N2—C36—C37—C38	0.10 (16)
C11—C10—C14—C5	−178.63 (13)	C30—C36—C37—C38	177.98 (13)
C13—C9—C15—N1	−111.82 (19)	N2—C36—C37—C40	−178.89 (13)
C12—C9—C15—N1	117.9 (2)	C30—C36—C37—C40	−1.0 (2)
Cl1—C9—C15—N1	2.37 (17)	C36—C37—C38—O6	0.37 (16)
C13—C9—C15—C16	65.4 (2)	C40—C37—C38—O6	179.32 (13)
C12—C9—C15—C16	−64.9 (2)	C36—C37—C38—C39	−178.35 (16)
Cl1—C9—C15—C16	179.60 (12)	C40—C37—C38—C39	0.6 (3)
N1—C15—C16—C17	0.40 (16)	C38—C37—C40—O7	173.17 (15)
C9—C15—C16—C17	−177.04 (14)	C36—C37—C40—O7	−8.1 (2)
N1—C15—C16—C19	178.26 (14)	C38—C37—C40—O8	−8.2 (2)
C9—C15—C16—C19	0.8 (2)	C36—C37—C40—O8	170.51 (13)
C15—C16—C17—O2	−0.56 (16)	C16—C15—N1—O2	−0.08 (15)
C19—C16—C17—O2	−178.34 (14)	C9—C15—N1—O2	177.56 (12)
C15—C16—C17—C18	176.92 (17)	C37—C36—N2—O6	−0.50 (15)
C19—C16—C17—C18	−0.9 (3)	C30—C36—N2—O6	−178.54 (11)
C17—C16—C19—O3	177.55 (15)	C16—C17—O2—N1	0.55 (16)
C15—C16—C19—O3	0.2 (2)	C18—C17—O2—N1	−177.50 (12)
C17—C16—C19—O4	−1.2 (2)	C15—N1—O2—C17	−0.28 (15)
C15—C16—C19—O4	−178.51 (13)	O3—C19—O4—C20	−1.2 (2)
C33—C22—C23—C24	0.4 (2)	C16—C19—O4—C20	177.50 (12)
C22—C23—C24—C25	−2.5 (2)	C21—C20—O4—C19	−161.22 (13)
C23—C24—C25—C32	1.7 (2)	C37—C38—O6—N2	−0.69 (15)
C35—C26—C27—C28	−0.7 (2)	C39—C38—O6—N2	178.32 (12)
C26—C27—C28—C29	−0.2 (2)	C36—N2—O6—C38	0.73 (14)
C27—C28—C29—C34	1.1 (2)	O7—C40—O8—C41	0.3 (2)
C24—C25—C32—C33	1.2 (2)	C37—C40—O8—C41	−178.28 (12)
C24—C25—C32—C31	−178.12 (13)	C42—C41—O8—C40	174.26 (12)